RESOURCE
https://doi.org/10.1038/s41593-020-00795-0

nature neuroscience

Single-cell transcriptomic analysis of the adult mouse spinal cord reveals molecular diversity of autonomic and skeletal motor neurons

Jacob A. Blum[1,2], Sandy Klemm[1,7], Jennifer L. Shadrach[3,7], Kevin A. Guttenplan[1,2], Lisa Nakayama[1], Arwa Kathiria[1], Phuong T. Hoang[1,4], Olivia Gautier[1,2], Julia A. Kaltschmidt[3], William J. Greenleaf[1,5,6] and Aaron D. Gitler[1]✉

The spinal cord is a fascinating structure that is responsible for coordinating movement in vertebrates. Spinal motor neurons control muscle activity by transmitting signals from the spinal cord to diverse peripheral targets. In this study, we profiled 43,890 single-nucleus transcriptomes from the adult mouse spinal cord using fluorescence-activated nuclei sorting to enrich for motor neuron nuclei. We identified 16 sympathetic motor neuron clusters, which are distinguishable by spatial localization and expression of neuromodulatory signaling genes. We found surprising skeletal motor neuron heterogeneity in the adult spinal cord, including transcriptional differences that correlate with electrophysiologically and spatially distinct motor pools. We also provide evidence for a novel transcriptional subpopulation of skeletal motor neuron (γ*). Collectively, these data provide a single-cell transcriptional atlas (http://spinalcordatlas.org) for investigating the organizing molecular logic of adult motor neuron diversity, as well as the cellular and molecular basis of motor neuron function in health and disease.

The CNS receives sensory input from its surroundings, integrates that information and then communicates with muscles and organs throughout the body to enact an appropriate response. Although a vast, interconnected network of neurons is responsible for processing information and planning motor behaviors, the transmission of signals from the CNS to peripheral muscles is controlled by one special and rare cell population: the spinal motor neuron.

Spinal motor neurons are unique because they reside in the CNS yet extend their axons far into the periphery to reach their innervation targets. Their activity is essential for virtually all skeletal and smooth muscle contractions in the body, controlling actions that range from the regulation of blood pressure and sweat secretion to the contraction of fast-twitch muscle fibers. Because of the vast diversity of muscular function within the body, motor neurons must tune their synaptic connections and electrophysiological properties to the unique features of the effector cells they control[1]. The intricate process of establishing motor neuron identity requires both cell-intrinsic and cell-extrinsic signaling during spinal cord development, culminating in the tightly controlled expression of transcription factors and cell signaling molecules that define motor circuits[2–4].

Considering their physiological importance, it is not surprising that spinal motor neuron dysfunction underlies human neuromuscular diseases. Indeed, spinal motor neuron degeneration is causally responsible for amyotrophic lateral sclerosis (ALS), spinal muscular atrophy and other rare neuromuscular disorders. In many of these diseases, certain populations of spinal motor neurons are selectively affected, whereas others are spared[5]. Defining the ground state for transcriptional differences between motor neuron subtypes in the adult will empower the analysis of molecular mechanisms that separate susceptible and resistant populations, leading to a better understanding of the molecular underpinnings of cell type vulnerability.

Despite their critical functional role, spinal motor neurons make up less than 0.4% of the total cells in the mammalian spinal cord. This rarity has made them notoriously difficult to transcriptionally characterize[6]. To overcome this challenge, we developed a motor neuron enrichment strategy using a fluorescent reporter mouse (Methods). This yielded a ~100-fold increase in representation of motor neuron nuclei over past efforts[7], enabling us to assess the transcriptional diversity of motor neurons in the adult spinal cord.

We performed single-nucleus RNA sequencing (snRNA-seq) on 43,890 nuclei from the adult mouse spinal cord, providing unprecedented single-cell resolution of the spinal motor system. This method allowed us to transcriptionally distinguish spinal motor neurons of the autonomic nervous system (visceral motor neurons) and somatic nervous system (skeletal motor neurons) based on many newly discovered marker genes. Foundational work in the field of spinal cord development has established the molecular logic of spinal neuron differentiation and target specification[3,8]. These efforts set the stage for the present study, in which we performed an unbiased analysis and validation of motor neuron diversity in the adult mouse spinal cord. We demonstrate that single-nucleus transcriptional profiling can provide key insights into the link between the brain and the body by defining the neuropeptides, transmitters and receptors that motor neurons use to communicate. Furthermore, this detailed characterization will enable the development of a broad range of molecular tools, including transgenic mice

[1]Department of Genetics, Stanford University School of Medicine, Stanford, CA, USA. [2]Stanford Neurosciences Graduate Program, Stanford University School of Medicine, Stanford, CA, USA. [3]Department of Neurosurgery, Stanford University School of Medicine, Stanford, CA, USA. [4]Department of Neurology and Neurological Science, Stanford University School of Medicine, Stanford, CA, USA. [5]Department of Applied Physics, Stanford University, Stanford, CA, USA. [6]Chan Zuckerberg Biohub, San Francisco, CA, USA. [7]These authors contributed equally: Sandy Klemm, Jennifer L. Shadrach. ✉e-mail: agitler@stanford.edu

and a roadmap for reprogramming stem cells into specific motor neuron subtypes, which will unlock genetic access to previously uncharacterized spinal motor neuron populations.

Single-nucleus transcriptional profiling of the adult mouse spinal cord

Because spinal motor neurons are so scarce, we enriched for motor neuron nuclei using a transgenic fluorescent reporter mouse[9]. This technique enabled us to selectively isolate cholinergic nuclei (*Chat*$^+$), a population that encompasses all motor neurons and several interneuron subtypes in the adult mouse spinal cord (Methods). Given the important role of non-cell autonomous mechanisms in neurodegeneration, we also isolated non-motor neuron cells, including interneurons, astrocytes, microglia and oligodendrocytes. In total, we transcriptionally profiled 43,890 nuclei from a collection of male, female and mixed cohorts of wild-type adult mice, with 20–40% of nuclei coming from motor neurons and 60–80% coming from other cells in the spinal cord (Fig. 1a). We used graph-based methods to cluster nuclei and then annotate cell types across clusters based on averaged expression of common marker genes, including genes encoding neurotransmitter signaling machinery (Fig. 1b,c and Methods). This approach enabled us to simultaneously characterize motor neurons, while also comparing their transcriptomes with other cells within the spinal cord, to find marker genes that are exclusively expressed in cell populations of interest. We assigned all profiled nuclei into seven broad categories: excitatory interneurons, inhibitory interneurons, cholinergic neurons, astrocytes, microglia, oligodendrocytes and endothelial cells (Fig. 1c, Extended Data Fig. 1a,b and Supplementary Table 1). Based on these categories, we estimate that ~30% (13,589 cells) of the profiled single-nucleus transcriptomes correspond to cholinergic neurons. This is a considerable improvement in representation over previous efforts[7] and provides unparalleled access to the transcriptional heterogeneity of spinal motor neurons. We provide an interactive web portal to access and search all of the spinal cord transcriptome data: http://spinalcordatlas.org.

Novel genetic markers distinguish autonomic and skeletal motor neurons

We next asked whether the observed transcriptional diversity of spinal motor neurons corresponds to functionally defined cell types, as in development (Fig. 1d). We computationally isolated and used graph-based clustering (Methods) to segregate all cholinergic neurons into 21 clusters (Fig. 1e). We annotated these subpopulations as skeletal motor neurons, cholinergic interneurons and visceral motor neurons (Fig. 1f) based on expression of known marker genes as well as expression patterns of uncharacterized genes in the publicly available Allen Mouse Spinal Cord Atlas[10]. Specifically, we identified cholinergic interneurons based on their expression of *Pax2* (ref. [11]) and visceral motor neurons (that are part of the autonomic nervous system) by their expression of neuronal nitric oxide synthase (*Nos1*$^+$)[12]. We performed double-label in situ hybridization with *Chat* and *Nos1* to confirm that *Nos1* is expressed specifically in the lateral autonomic columns of the thoracic and sacral spinal cord—where visceral motor neurons are located (Extended Data Fig. 1c,d).

We hypothesized that the remaining three clusters represented skeletal motor neurons—a broad cell population with no known genetic markers that distinguish them from visceral motor neurons. To test this hypothesis, we examined the Allen Mouse Spinal Cord Atlas[10] for expression of two genes that are highly expressed in those clusters: *Bcl6* and *Tns1*. Indeed, in contrast to ubiquitous (*Actb*) and pan-neuronal (*Syn1*) transcripts, which show broad expression in transverse sections, it is apparent that *Bcl6* and *Tns1* are strongly expressed in small- and large-diameter neurons in the ventral horn of the spinal cord (Extended Data Fig. 2a–d). Future studies will investigate the expression patterns of these putative markers in greater depth, but this pattern is consistent with skeletal motor neurons. Our classification of skeletal and visceral motor neurons differs from a previous study, which postulated that two other genes, *Fbn2* and *Zeb2*, were novel markers specifically expressed in α motor neurons[13]. Instead, our transcriptional data indicate that that *Zeb2* and *Fbn2* are absent from skeletal motor neuron clusters (Extended Data Fig. 1e,f), the latter of which we confirmed by multiplexed *Chat*/*Fbn2* in situ hybridization (Extended Data Fig. 1g). Thus, these new transcriptional profiles reveal dozens of possible new marker genes that reliably distinguish skeletal motor neurons from other cells in the spinal cord. (Fig. 1g and Supplementary Table 2a).

Single-nucleus transcriptomics reveals diversity within the autonomic nervous system

Unlike skeletal motor neurons, which control voluntary movement, visceral motor neurons in the spinal cord control the activity of involuntary smooth muscles responsible for regulating homeostatic processes throughout the body. These cells are part of the sympathetic nervous system, whereas similar cells in the brain stem are part of the parasympathetic nervous system[12]. These sympathetic visceral motor neurons are developmentally very closely related to skeletal motor neurons[14,15] but do not innervate muscle fibers directly. Instead, they project from the lateral autonomic column of the spinal cord and synapse onto the peripheral ganglia in the sympathetic chain that control smooth muscle contraction (Fig. 2a)[12]. Neurons of the autonomic nervous system innervate nearly every organ in the body and, thus, have different functional requirements to fit the needs of each peripheral target (Fig. 2b). Could these functional differences be encoded by transcriptional heterogeneity?

The sympathetic nervous system is organized along the rostral–caudal axis of the spinal cord, such that visceral motor neurons that control the same organs are coarsely grouped near one another within the spinal cord (Fig. 2b). Intriguingly, past electrophysiological studies uncovered heterogeneity among visceral motor neurons with respect to their membrane properties, responsiveness to neurotransmitters[16] and sensitivity to hormones such as dopamine[17] and noradrenaline[18]. This evidence strongly suggests that the

Fig. 1 | Motor neuron enrichment and single-nucleus transcriptional analysis of the adult mouse spinal cord uncovers skeletal and visceral motor neuron markers. a, Workflow for cholinergic nucleus enrichment and snRNAseq: GFP$^+$ and TdTomato$^+$ cells were mixed at a ratio between 1:3 and 2:3. Plot shows the distribution of canonical cell types with their proportional representation. FACS was used to select appropriate proportion of singlet DAPI$^+$GFP$^+$tdTomato$^-$ nuclei. **b**, UMAP of clustered snRNA-seq data from 43,890 transcriptomes. **c**, Average expression levels per cluster for marker genes of each canonical cell population. Cell type labels based on expression patterns of marker genes. **d**, Schematic depicting expected cholinergic cell types in the spinal cord. Visceral motor neurons (blue) innervate sympathetic ganglia; skeletal motor neurons (green) directly innervate muscle fibers; and cholinergic interneurons (red) innervate motor neurons and other cells. **e**, UMAP with graph-based clustering of all cholinergic neurons reveals 21 clusters. **f**, Ranked expression of known marker genes *Pax2* (interneurons) and *Nos1* (visceral motor neurons), as well as marker gene *Anxa4* (skeletal motor neurons), by cluster. Cell labels were assigned hierarchically by expression levels of *Pax2*, *Nos1* and *Bcl6* and are reported below each plot. Cholinergic interneuron clusters that also express *Nos1* are denoted with asterisk (*). **g**, Enriched differentially expressed genes for cholinergic interneurons, skeletal motor neurons and visceral motor neurons. Dot size is proportional to the percent of each cluster expressing the marker gene, whereas blue color intensity is correlated with expression level. All expression values were log normalized in Seurat[50]. IN, interneuron; MN, motor neuron.

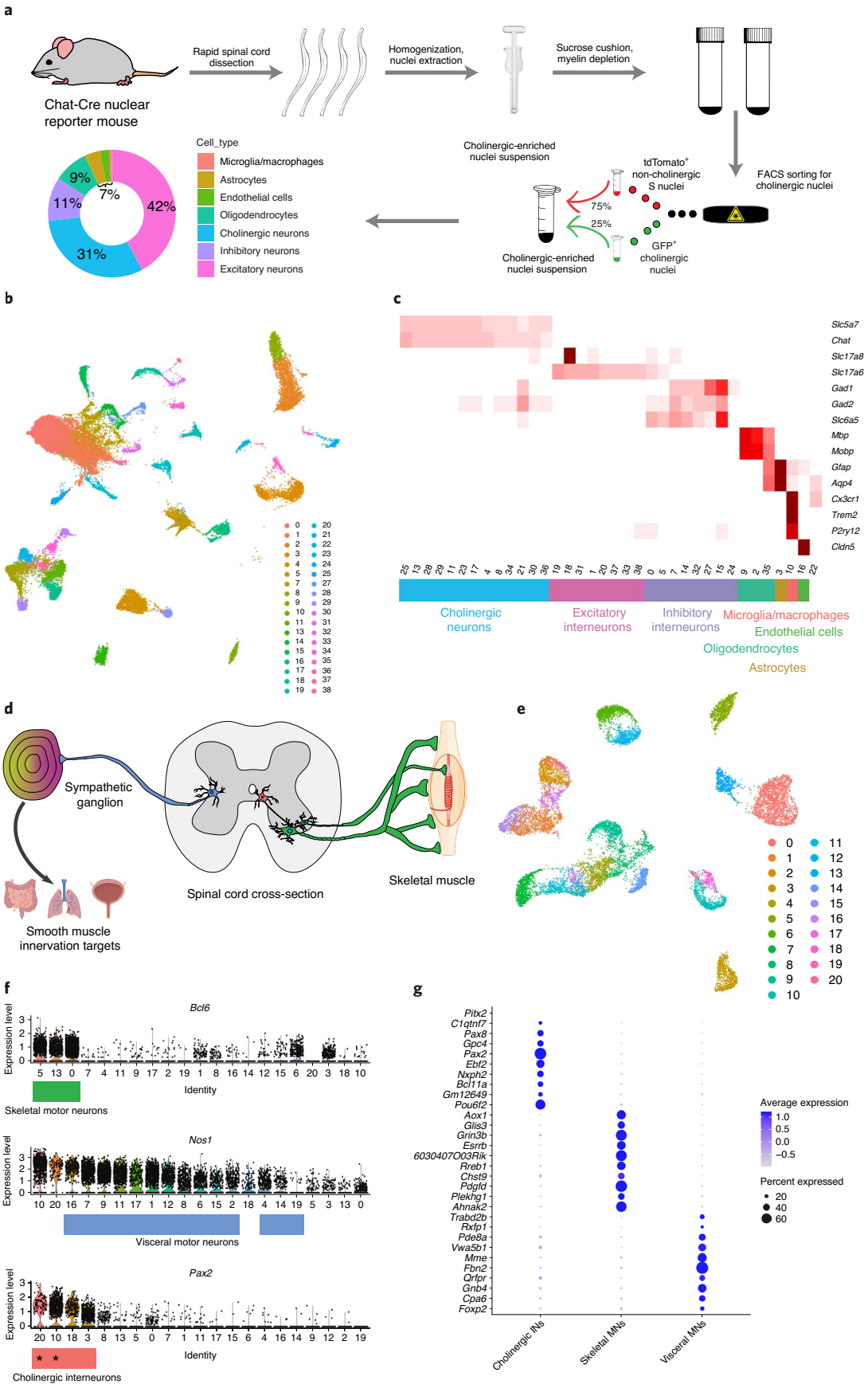
a
Chat-Cre nuclear reporter mouse
Rapid spinal cord dissection
Homogenization, nuclei extraction
Sucrose cushion, myelin depletion
FACS sorting for cholinergic nuclei
tdTomato+ non-cholinergic S nuclei
GFP+ cholinergic nuclei
75%
25%
Cholinergic-enriched nuclei suspension
Cholinergic-enriched nuclei suspension
Cell_type
Microglia/macrophages
Astrocytes
Endothelial cells
Oligodendrocytes
Cholinergic neurons
Inhibitory neurons
Excitatory neurons
9%
7%
11%
42%
31%
b
c
Slc5a7
Chat
Slc17a8
Slc17a6
Gad1
Gad2
Slc6a5
Mbp
Mobp
Gfap
Aqp4
Cx3cr1
Trem2
P2ry12
Cldn5
Cholinergic neurons
Excitatory interneurons
Inhibitory interneurons
Microglia/macrophages
Endothelial cells
Oligodendrocytes
Astrocytes
d
Sympathetic ganglion
Spinal cord cross-section
Skeletal muscle
Smooth muscle innervation targets
e
f
Bcl6
Expression level
Identity
Skeletal motor neurons
Nos1
Visceral motor neurons
Pax2
Cholinergic interneurons
g
Pitx2
C1qtnf7
Pax8
Gpc4
Pax2
Ebf2
Nxph2
Bcl11a
Gm12649
Pou6f2
Aox1
Glis3
Grin3b
Esrrb
6030407O03Rik
Rreb1
Chst9
Pdgfd
Plekhg1
Ahnak2
Trabd2b
Rxfp1
Pde8a
Vwa5b1
Mme
Fbn2
Qrfpr
Gnb4
Cpa6
Foxp2
Cholinergic INs
Skeletal MNs
Visceral MNs
Average expression
Percent expressed

visceral motor system contains physiologically distinct subpopulations, but the overarching molecular logic underlying the sympathetic nervous system remains unresolved.

We hypothesized that transcriptomic clusters might reflect distinct populations of visceral motor neurons that innervate specific peripheral targets, are selectively responsive to hormones[17] and/or use distinct classes of neuropeptides in transmitting signals to peripheral ganglia[19]. To test these hypotheses, we subclustered all visceral motor neurons. By limiting the diversity of cell types that are concurrently analyzed and subclustering along principal axes of variation specific to visceral motor neurons, we resolved 16 transcriptionally distinct subpopulations (Fig. 2c). We identified marker genes that are, according to the Allen Spinal Cord Atlas[10], expressed in the adult mouse lateral autonomic column of the spinal cord and are significantly enriched in at least one of the 16 visceral motor neuron populations (Supplementary Table 3). For each marker gene, we estimated a normalized spatial density of expressing cells along the rostral–caudal spinal cord using data from the Allen Spinal Cord Atlas (Methods). We then estimated the positional distribution of cells within each visceral motor neuron cluster as an average of these spatial cell distributions, weighted by the relative expression levels of the marker genes within each cluster (Methods). Although most clusters showed no strong spatial bias along this axis, clusters 3, 7 and 10 showed a clear enrichment in the sacral spinal cord (Extended Data Fig. 3a).

To confirm these findings, we selected several genes that are enriched in distinct clusters (*Rxfp1*, *Nts*, *Cdh8*, *Piezo2*, *Creb5* and *Fbn2*) and performed in situ hybridizations on sections every 600 µm along the rostral–caudal axis of the adult spinal cord (Fig. 2d and Extended Data Fig. 3b). The results of this analysis were striking: we confirmed that *Rxfp1* (clusters 3 and 7) is expressed exclusively in the sacral spinal cord (Fig. 2d and Extended Data Fig. 3c,d). Among other roles, sacral visceral motor neurons modulate sexual function—an intriguing finding given that male and female sexual organs release relaxin family peptides[20,21], which bind to Rxfp1. We provide *Rxfp1* as an example for how these sequencing data can reveal functionally relevant receptor expression, and there are other highly specific hormone receptor genes in distinct clusters (Table 1). We speculate that differentially expressed hormone receptor expression among visceral motor populations might be tuned to central pre-synaptic inputs and/or peripheral innervation targets.

We found preganglionic clusters to be highly transcriptionally divergent, with many individual markers capable of distinguishing specific clusters (Fig. 2e). Strikingly, the most common subtype of visceral motor neurons (cluster 0) expresses high levels of *Neurotensin* (*Nts*) and is, therefore, neurotensinergic. These neurotensinergic motor neurons are distributed throughout the thoracic and sacral lateral autonomic columns (Fig. 2d). *Nts* expression was remarkably binary, with Nts^{on} and Nts^{off} visceral motor neurons frequently observed directly adjacent to one another in transverse sections (Fig. 2f). Neurotensin is a 13-amino-acid peptide, which, when injected into rats, causes potent inhibition of sympathetic circuits that regulate blood pressure, heart rate and inspiratory drive, among other effects on the sympathetic nervous system[22]. Remarkably, although *Nts* is clearly involved in regulating sympathetic nervous function, its role in spinal preganglionic motor neurons has not been studied. We present strong evidence that *Nts* expression is a defining feature of preganglionic motor identity and provide the transcriptional roadmap for more detailed future characterization.

Because several studies showed that hormones, neuropeptides and monoaminergic signaling play a crucial role in the sympathetic nervous system[17–23], we were interested in differentially expressed genes that would affect those pathways. We observed remarkable specificity of neuropeptides and receptors—as well as neurotransmitter receptors—across visceral motor neuron clusters (Fig. 2f and Table 1). Adrenergic receptors, for example, show a remarkable degree of expression specificity in our single-nucleus sequencing data. Type I adrenergic receptor *Adra1a* is expressed in clusters 3 and 7, which we previously determined to correspond to sacral autonomic motor neurons (Fig. 2d). On the other hand, type II adrenergic receptor *Adra2a* is expressed at low levels in all visceral populations (Extended Data Fig. 3e). We also found highly specific expression of neuroactive peptide precursors, such as *Penk* and *Sst* in cluster 3 (Table 1). Together, these findings suggest that the repertoire of neuropeptide and hormone receptor expression is an organizing logic within the sympathetic preganglionic motor system.

Transcriptional characterization of cholinergic inhibitory neurons

Cholinergic interneurons are a rare cell population marked by *Pax2* expression[11]. They play key roles in the circuits underlying locomotor behaviors[24] (Fig. 2g). Subclustering revealed eight distinct transcriptional populations of cholinergic interneurons (Fig. 2h), including clusters 2, 3, 5, 6 and 7 that express high levels of *Nos1*, which is traditionally considered to be a marker of the autonomic nervous system in the spinal cord[12] (Fig. 2i). It remains to be determined whether these $Nos1^{+}$ cholinergic cells are interneurons or, instead, a preganglionic motor neuron population that projects into the periphery but also expresses the interneuron marker *Pax2*. A subset of this population of cells (clusters 2, 3 and 6) also expresses higher levels of *Piezo2*, a mechanosensitive ion channel involved in proprioception, than any other population in the adult spinal cord (Supplementary Table 2a). We performed in situ hybridization to demonstrate that cholinergic, *Piezo2*-high cells have large cell bodies and predominantly localize just lateral of the central canal (Extended Data Fig. 3f). Notably, the localization and size of these cholinergic interneurons strongly resemble previously identified $Pitx2^{-}$ 'C3' cells[25].

In contrast, clusters 0 and 1 do not express *Nos1* but instead express *Pitx2*—an established marker of partition cells[25,26] (Fig. 2j). Partition cells are a subset of cholinergic interneurons that make direct cholinergic synapses with motor neuron soma and proximal dendrites. These synapses, referred to as 'C boutons', modulate motor neuron excitability during locomotor activity[25]. There

Fig. 2 | Single-nucleus transcriptomics reveals immense diversity within the autonomic nervous system and partition cells. a, Schematic illustrating the position of sympathetic visceral motor neurons (blue) in the lateral autonomic column of the spinal cord. **b**, Diagram adapted from Espinosa-Medina et al. showing innervation targets of the sympathetic nervous system[12]. **c**, UMAP with 16 visceral motor neuron subclusters. Inset shows all cells from Fig. 1e that were subclustered. **d**, Frequency of visceral motor neuron subpopulations ($Rxfp1^{+}$ and Nts^{+}) along the rostral–caudal axis of the spinal cord. Individual data points for total visceral motor neurons are shown with filled circles, whereas marker gene-positive cell numbers are shown with filled triangles. $n = 3$ biologically independent animals. **e**, Novel marker genes for each cluster of visceral motor neurons. **f**, Representative in situ hybridization of *Chat*, *Nts and Fbn2* demonstrating *Nts* expression in visceral motor neurons. Scale bar, 200 µm and 20 µm (inset). $n = 3$ biologically independent animals. **g**, Schematic showing cholinergic interneuron innervation of skeletal motor neurons as demonstrated previously[25]. **h**, UMAP with graph-based clustering labels for cholinergic interneurons. Inset shows all cells from Fig. 1e that were subclustered. **i**, Novel marker genes for cholinergic interneuron clusters are identified. **j**, Expression of *Pitx2* in cholinergic interneuron populations, overlaid on UMAP projection from **h**. Clusters 0 and 1 are *Pitx2* positive. All expression values were log normalized in Seurat[50]. Dot size is proportional to the percent of each cluster expressing the marker gene, whereas blue color intensity is correlated with expression level in **e** and **i**.

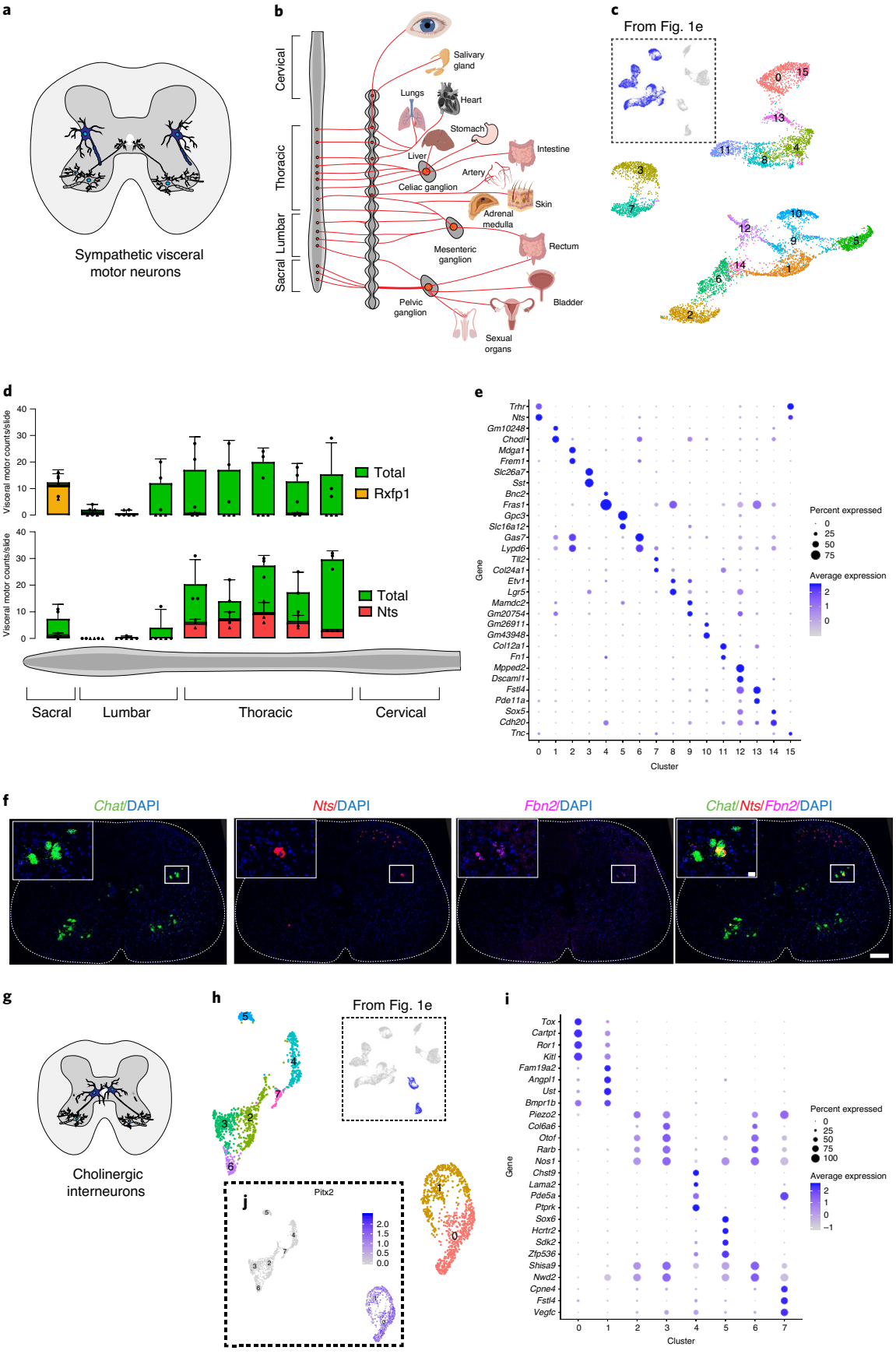
a
Sympathetic visceral motor neurons
b
Cervical
Thoracic
Sacral Lumbar
Salivary gland
Lungs
Heart
Stomach
Liver
Intestine
Artery
Celiac ganglion
Skin
Adrenal medulla
Mesenteric ganglion
Rectum
Pelvic ganglion
Bladder
Sexual organs
c
From Fig. 1e
d
Visceral motor counts/slide
Total
Rxfp1
Nts
Sacral
Lumbar
Thoracic
Cervical
e
Gene
Cluster
Percent expressed
Average expression
f
Chat/DAPI
Nts/DAPI
Fbn2/DAPI
Chat/Nts/Fbn2/DAPI
g
Cholinergic interneurons
h
From Fig. 1e
Pitx2
i
Gene
Cluster
Percent expressed
Average expression
j
Pitx2

Table 1 | Differentially expressed signaling machinery genes among visceral motor neuron clusters

	Gene product	Diff. expressed cluster
Serotonergic		
Htr2c	Serotonin receptor 2	**2, 4**
Htr1f	Serotonin receptor 1	**3**
Htr2a	Serotonin receptor 2	**13**
Adrenergic		
Adra1a	Adrenergic receptor 1	**3, 7**
Dopaminergic		
Drd2	Dopamine receptor 2	**11**
Hormone signaling		
Prlr	Prolactin receptor	**0, 15**
Trhr	Thyrotropin-releasing hormone receptor	**0, 15**
Trhde	Thyrotropin-releasing hormone-degrading enzyme	**7, 11**
Rxfp1	Relaxin family peptide receptor 1	**3, 7**
Ghr	Growth hormone receptor	**11**
Gfra1	GDNF family receptor	**3, 5, 14**
Qrfpr	Orexigenic neuropeptide QRFP receptor	**0, 13, 15**
Hcrtr2	Orexin receptor type II	**3, 5, 15**
Tacr1	Tachykinin (substance P) receptor 1	**2, 3**
Opioid signaling		
Penk	Enkephalin	**3**
Oprm1	Opioid receptor mu 1	**9**
Neuropeptide (other)		
Sst	Somatostatin	**3**
Nts	Neurotensin	**0, 15**
Cartpt	Cart peptide	**1, 9**
Misc. signaling		
Lifr	Lif receptor	**4, 5**
Tnc	Tenascin	**15**
Tnr	Tenascin receptor	**11, 13, 15**

All genes listed show differential enrichment in one cluster compared with all others (Wilcoxon rank sum test, $P_{adj} < 0.01$ (Bonferroni) and $\log_2$ FC > 0.5).

is a robust transcriptional signature that separates partition cells from other cells in the spinal cord (Supplementary Table 2a,d). Of particular interest is *Gldn*, a gene that is selectively expressed in the cluster of cholinergic *Pitx2*$^+$ cells that have previously been identified as partition cells (Extended Data Fig. 3g). Mutations in *GLDN* cause lethal congenital contracture syndrome, a crippling neurodegenerative disease in which joints become permanently fixed in a bent or straight position[27]. Future studies should seek to examine if *GLDN* mutations affect partition cells.

Elegant viral tracing studies have delineated partition cells into ipsilaterally and contralaterally projecting populations that make exquisitely specific synaptic connections with motor neurons[28]. We found a parallel transcriptional bifurcation in partition cells, which segregate into two main clusters that are genetically delineated by many differentially expressed genes. One example is *Nrxn3*, which encodes a cell adhesion molecule responsible for establishing synaptic specificity (Extended Data Fig. 3h). Further in vivo experiments will be necessary to definitively show whether these transcriptionally distinct populations correspond to ipsilateral and contralateral projecting populations and whether *Nrxn3* plays a functional role in partition circuit assembly and maintenance. By identifying these populations in our data, we present a detailed molecular characterization of partition cells and reveal several novel marker genes of cholinergic interneurons cell classes.

Identification of novel α and γ motor neuron markers

Traditionally, skeletal motor neurons have been defined based on their muscle innervation target[4,29], developmental lineage[30], morphology and electrophysiological properties[5,31]. They are classified as α, β and γ spinal motor neurons (Fig. 3a). α motor neurons directly innervate extrafusal muscle fiber neuromuscular junctions. In contrast, γ motor neurons innervate intrafusal muscle spindles[32]. We identified skeletal motor neurons by *Tns1/Bcl6* expression (as above; Methods) and then subclustered them (Fig. 3b).

To identify putative α and γ motor neurons, we examined expression patterns of the few robust genetic markers of these populations that have been confirmed in adult animals[32–35] (Fig. 3c). Clusters 0, 2 and 6 express high levels of *Htr1d* and low levels of *Rbfox3* and *Spp1* (Fig. 3c and Supplementary Table 2e), suggesting that they represent γ motor neurons. The remaining clusters minimally express *Htr1d*, suggesting that they represent α motor neurons (Fig. 3c). We calculated differential gene expression between putative α and γ motor neuron clusters, yielding a collection of novel markers of each population (Fig. 3d). To validate a putative marker of γ motor neurons (*Npas1*), we performed multiplexed in situ hybridization with the canonical γ markers *Htr1d* and *Chat* in the adult spinal cord. These experiments demonstrate robust co-expression in cholinergic cells in the ventral horn (Fig. 3e). Similarly, we performed in situ hybridization comparing expression of *Chat*, a novel α marker (*Vipr2*), and an established marker of α motor neurons (*Rbfox3*) to confirm that *Vipr2* is expressed solely in α motor neurons (Fig. 3e and Extended Data Fig. 4a,b). Additionally, *Vipr2* and *Htr1d* have non-overlapping expression patterns in *Chat*$^+$ cells (Extended Data Fig. 4c), as do *Npas1* and *Rbfox3* (Extended Data Fig. 4d). As a final confirmation,

Fig. 3 | Transcriptional differences between α and γ motor neurons. a, Transverse schematic illustrating the position of skeletal motor neurons (blue) in the ventral horn of the spinal cord. γ motor neurons are small and innervate intrafusal muscle fibers. α motor neurons are large and innervate extrafusal fibers. **b**, UMAP with 11 subclustered skeletal motor neuron populations. Inset shows all cells from Fig. 1e that were subclustered. **c**, Average expression of known γ marker *Htr1d* and α markers *Rbfox3* and *Spp1* by cluster. **d**, Heat map with average expression by cluster of differentially expressed genes in α and γ populations. Differentially expressed genes between γ and α populations. **e**, Representative in situ hybridization against *Chat/Htr1d/Npas1* and *Chat/Rbfox3/Vipr2* in transverse lumbar spinal cord sections. Arrowheads indicate γ motor neurons in both images. Scale bars, 200 µm (overview) and 50 µm (inset). $n = 4$ biologically independent animals. **f**, Transverse schematic illustrating γ motor neurons (blue) innervating intrafusal muscle fibers. Inset shows all cells from Fig. 3b that were subsequently subclustered. **g**, Heat map showing fundamental subdivision between γ and γ* motor neurons, hierarchically clustered by expression of highly variable genes among all classes of γ motor neurons (Methods). **h**, Differentially expressed membrane receptors between two main populations of γ motor neurons, as well as novel markers that delineate them. **i**, Representative in situ hybridization against *Htr1d/Plch1/Creb5* in transverse lumbar spinal cord. *Plch1* and *Creb5* are expressed reciprocally in *Htr1d*$^+$ cells and represent γ and γ* motor neurons. Arrowheads demarcate *Creb5*$^+$ γ motor neurons, and * indicates γ* motor neurons. $n = 5$ biologically independent animals. All differential expression was calculated using Wilcoxon rank sum test and adjusted for multiple comparisons (Bonferroni method) ($P_{adj} < 0.01$ and $\log_2$ FC > 0.5). All expression values were log normalized in Seurat[50]. Scale bars, 50 µm.

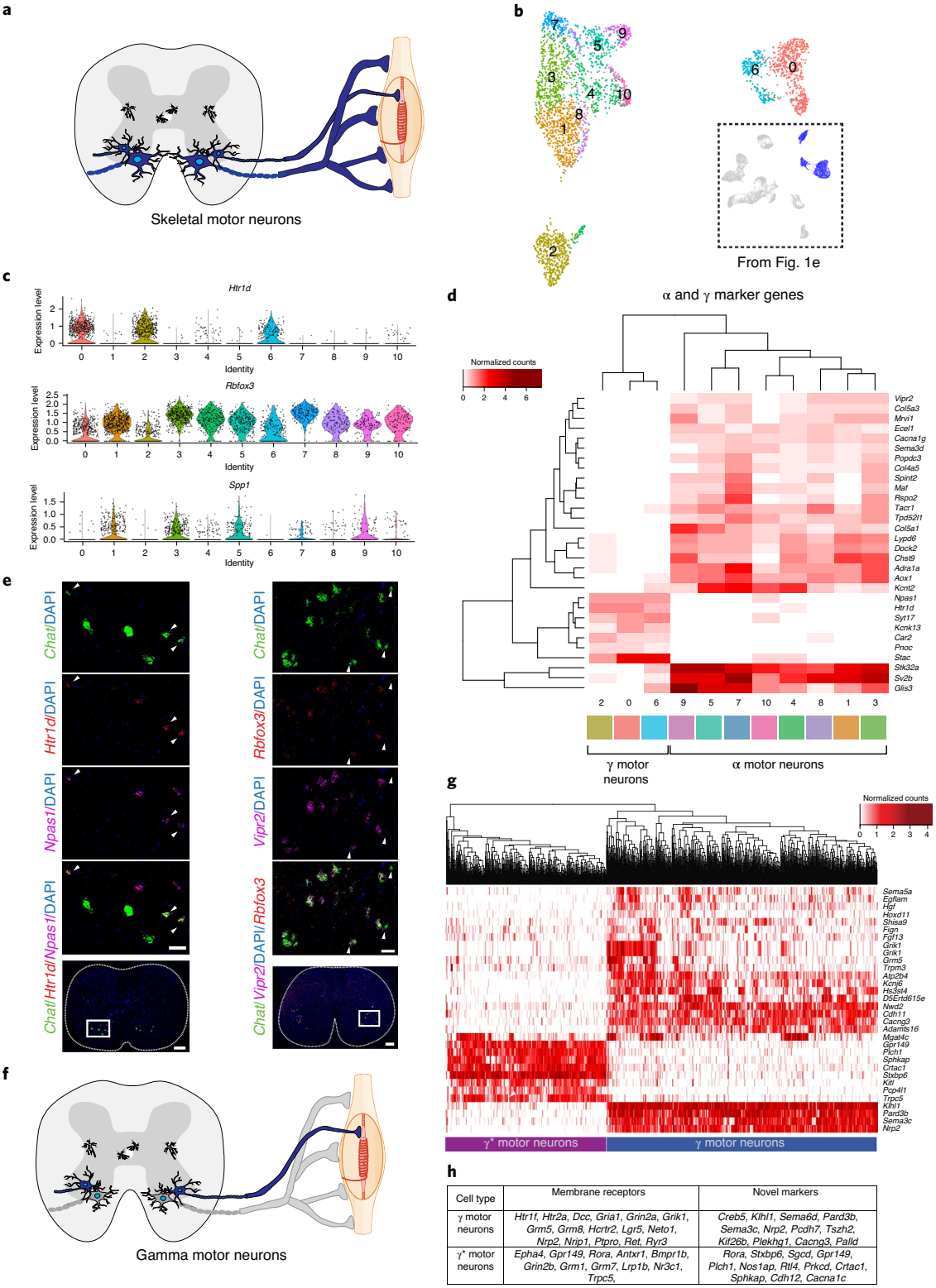

Cell type	Membrane receptors	Novel markers
γ motor neurons	*Htr1f, Htr2a, Dcc, Gria1, Grin2a, Grik1, Grm5, Grm8, Hcrtr2, Lgr5, Neto1, Nrp2, Nrip1, Ptpro, Ret, Ryr3*	*Creb5, Klhl1, Sema6d, Pard3b, Sema3c, Nrp2, Pcdh7, Tszh2, Kif26b, Plekhg1, Cacng3, Palld*
γ* motor neurons	*Epha4, Gpr149, Rora, Antxr1, Bmpr1b, Grin2b, Grm1, Grm7, Lrp1b, Nr3c1, Trpc5,*	*Rora, Stxbp6, Sgcd, Gpr149, Plch1, Nos1ap, Rtl4, Prkcd, Crtac1, Sphkap, Cdh12, Cacna1c*

we show that *Vipr2* and *Npas1* are expressed in reciprocal populations of motor neurons in the ventral horn (Extended Data Fig. 4e). Notably, all existing α motor neuron markers are insufficient on their own to distinguish them from other cells in the spinal cord. In contrast, *Vipr2* is expressed exclusively in α motor neurons. Together, these results provide a robust molecular basis for distinguishing α and γ motor neurons using newly described genetic markers.

Transcriptional profiles of γ spinal motor neurons reveal two highly divergent motor neuron types

γ motor neurons innervate intrafusal muscle fibers, which maintain the tension required for skeletal muscle to function properly (Fig. 3f). Hierarchical clustering of γ motor neuron marker genes (*Htr1d*$^+$) revealed two main clusters (Fig. 3g), which are distinguished by the expression of many individual transcripts (Fig. 3h). When clustering is taken to an even more granular level, segmenting γ motor neurons into four distinct populations (Extended Data Fig. 5a,b); however, the majority of variation is captured by dividing them into two populations. We noticed that many of the genes enriched in the *Stxbp6*$^+$ population are also expressed more broadly by α motor neurons (Extended Data Fig. 5c,d). We named this new population γ* (pronounced 'gamma star'), whereas all other *Htr1d*$^+$ cells are canonical γ motor neurons. We can reliably distinguish γ from γ* by reciprocal expression of either *Stxbp6* or *Plch1* (γ*) and *Creb5* or *Pard3b* (γ), both in our single-cell dataset (Extended Data Fig. 5e–h), and by in situ hybridization (Fig. 3i and Extended Data Fig. 5i,j). Owing to the extensive number of differentially expressed genes that separate γ from γ*, as well as the lack of an intermediate population between them that would suggest that they are two functional 'states' of γ motor neurons, we hypothesize that these cell types represent a fundamental subdivision of the fusimotor system. However, future work will be necessary to conclusively determine if this subdivision corresponds to transient 'activity states' of γ motor neurons or developmentally and functionally distinct populations of cells.

One kind of skeletal motor neuron that has been defined physiologically and anatomically, but not yet transcriptionally, is the β motor neuron. This cell type innervates both intrafusal and extrafusal fibers and, therefore, has properties of both α and γ motor neurons[36]. Could γ* actually correspond to this historically elusive and long-sought skeletal motor neuron subtype? We present a list of novel markers that differentiate the γ and γ* populations (Fig. 3h), which will enable a more detailed exploration in the future.

Transcriptional analysis of α motor neurons reveals motor pools

During development, motor neurons require cell-intrinsic and cell-extrinsic cues that coordinate expression of transcription factors and cell adhesion molecules[3,4]. This molecular cascade enables α motor neurons to form into groups, known as motor pools, that cluster alongside one another in the spinal cord and collectively innervate the extrafusal fibers of distinct muscles[33] (Fig. 4a). Owing to a vast heterogeneity in muscle location throughout the body and the types of muscle contractions required for coordinated movement, mature α motor neurons display substantial functional differences[37–39]. However, a priori, it was unknown whether electrophysiological subtypes of α motor neurons with specific innervation targets express different transcriptional programs.

Foundational studies strongly suggest that motor neuron target specificity arises from transcriptional heterogeneity[3] during development, but whether these differences persist into adulthood is unknown. We subclustered the α motor neuron transcriptomes (as above; Methods and Fig. 4b). This analysis revealed 12 clusters. Most α motor neurons fall in one large population that consists of clusters 0, 1 and 4. Other clusters diverge transcriptionally from this main population and express specific distinguishing markers (Fig. 4c). Cluster 3 expresses *Cpne4* and *Fign* specifically (Fig. 4c and Supplementary Table 2f)—genes that were recently shown to be highly expressed in intrinsic foot (IF) motor neurons during development[37]. Furthermore, clusters 7 and 8 express high levels of *Sema3e* (Fig. 4c), which, within the developing lumbar spinal cord, is a specific genetic marker for gluteus maximus (GLUT)-innervating motor neurons[40], as well as shoulder-innervating motor neurons in the cervical spinal cord[41]. *Sema3e* encodes a protein that, together with its receptor PlexinD1, contributes to synaptic specificity between sensory and motor neurons in that pool[40,41]. These findings raise the hypothesis that single-nucleus transcriptomics is sufficient to distinguish subpopulations of α motor neurons that, in the adult mouse specifically, innervate unique muscle groups.

To test whether the α motor neuron clusters that we identified by transcriptomics correspond to functionally defined motor pools, which collectively innervate a specific muscle, we performed intramuscular injections of fluorescently conjugated cholera toxin beta (CTB) subunit—a recombinant protein that is taken up by motor neuron axon terminals and transported retrogradely to the cell body[42]. By performing simultaneous CTB labeling and in situ hybridization against candidate marker genes for a given population, we are able to perform whole-transcriptome characterization

Fig. 4 | α motor neuron pool, position and electrophysiological subtype reflect transcriptional differences. a, Transverse schematic shows α motor neurons (blue) innervating extrafusal muscle fibers. **b**, UMAP with 12 subclustered α motor neuron populations. Inset shows all α motor neurons from Fig. 3b that were subclustered. **c**, Novel marker gene expression across α motor neuron subpopulations. Dot size is proportional to the percent of each cluster expressing the marker gene, whereas blue color intensity is correlated with expression level. **d**, Representative in situ hybridization against novel (*Hcrtr2*) and known (*Cpne4*) instrinsic foot (IF) motor pool markers in longitudinal sections, overlaid with CTB-labeled cells that innervate the gluteus maximus (GLUT) and IF. $n = 5$ (IF) and 4 (GLUT) biologically independent animals. **e**, Proportion of CTB-labeled cells from GLUT and IF that are labeled with *Hcrtr2* and *Cpne4* shows novel and known markers that selectively label the IF motor pool. $n = 5$ (IF) and 4 (GLUT) biologically independent animals. **f**, Schematic illustrating SF (blue), FR (purple) and FF (red) α motor neuron populations innervating type I, type IIa and type IIb fibers, respectively. **g**, Heat map showing all α motor neurons, hierarchically clustered and colored by expression of differentially expressed genes between fast (*Chodl*$^+$) and slow (*Sv2a*$^+$) α motor neurons, shows three cell populations corresponding to SF, FR and FF motor neurons. Red and blue bars show gene modules enriched in fast- and slow-firing α motor neurons, respectively. **h**, Representative in situ hybridization in longitudinal sections against novel (*Kcnq5* and *Prkcd*) and known (*Chodl* and *Sv2a*) fast- and slow-firing motor neuron markers, respectively. Images show CTB-labeled cells that innervate a muscle with predominantly fast-twitch fibers (TA) and slow-twitch fibers (SOL). $n = 5$ (TA) and 4 (SOL) biologically independent animals. **i**, Proportion of CTB-labeled cells from TA and SOL that are labeled with *Chodl* and *Kcnq5*. The TA has a significantly larger proportion of *Chodl*$^+$ and *Kcnq5*$^+$ cells than the SOL, although *Kcnq5*$^+$ cells are significantly less frequently found in both populations. $n = 5$ (TA) and 4 (SOL) biologically independent animals. Adjusted P (P_{adj}) = 0.0197 (*Chodl*) and $P = 0.0262$ (*Kcnq5*). **j**, Proportion of CTB-labeled cells from TA and SOL that are labeled with *Sv2a* and *Prkcd*. The SOL pool has a significantly larger proportion of *Prkcd*$^+$ and *Sv2a*$^+$ cells than the TA. $n = 5$ (TA) and 4 (SOL) biologically independent animals. All differential expression calculated using Wilcoxon rank sum test and adjusted for multiple comparisons (Bonferroni method) ($P_{adj} < 0.01$ and $\log_2$ FC > 0.5). All expression values were log normalized in Seurat[50]. Scale bars, 50 μm (**h**) and 75 μm (all others). One-way ANOVA with post hoc Sidak multiple comparison test between same-gene conditions. *$P < 0.05$, **$P < 0.01$, ***$P < 0.001$ and ****$P < 0.0001$. Error bars are s.e.m.

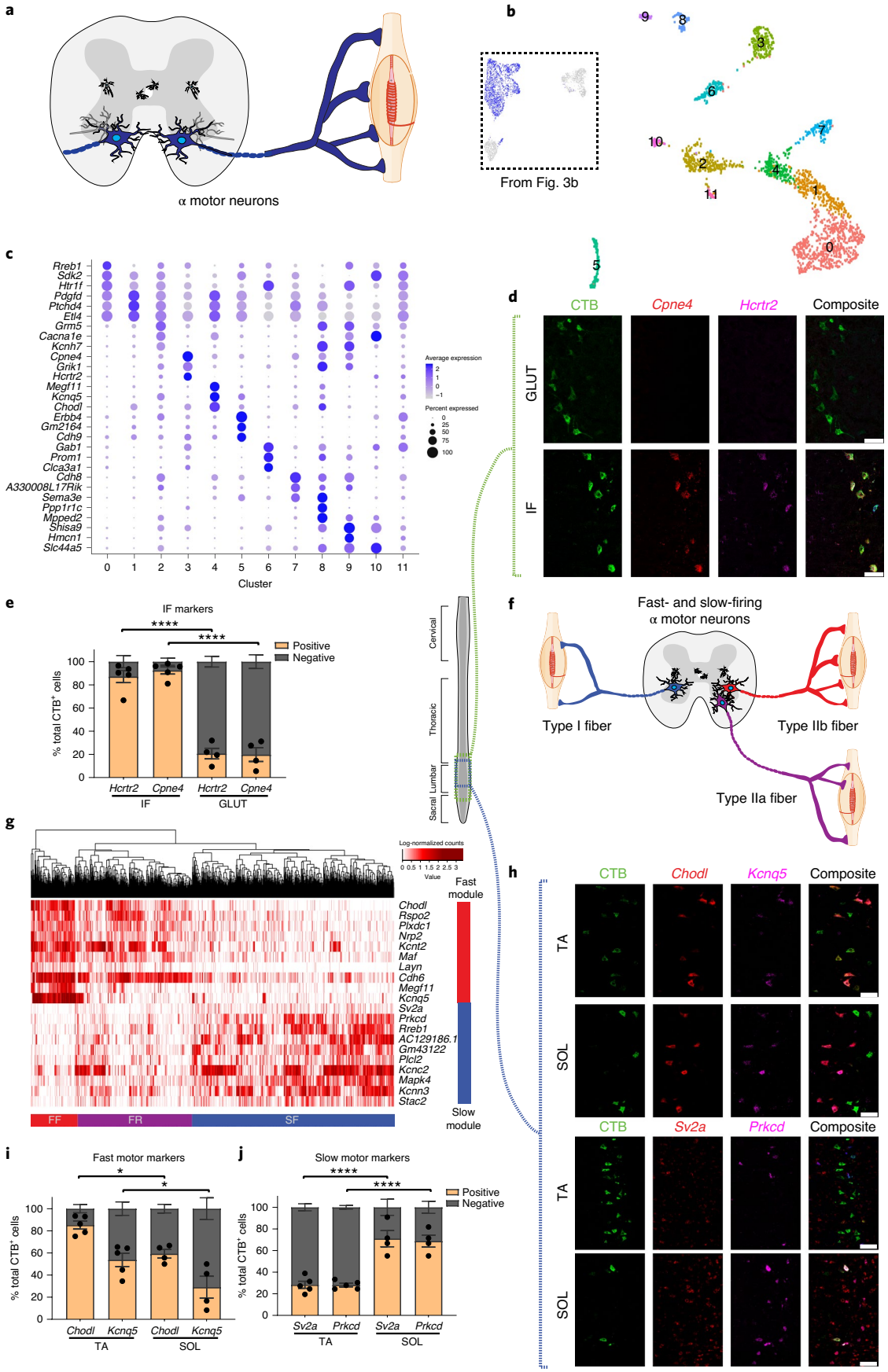
a
α motor neurons
b
From Fig. 3b
c
Cluster
Average expression
Percent expressed
d
CTB
Cpne4
Hcrtr2
Composite
GLUT
IF
e
IF markers
Positive
Negative
% total CTB+ cells
Hcrtr2 Cpne4 Hcrtr2 Cpne4
IF GLUT
Cervical
Thoracic
Lumbar
Sacral
f
Fast- and slow-firing α motor neurons
Type I fiber
Type IIb fiber
Type IIa fiber
g
Log-normalized counts
Fast module
Slow module
FF FR SF
h
CTB
Chodl
Kcnq5
Composite
TA
SOL
CTB
Sv2a
Prkcd
Composite
TA
SOL
i
Fast motor markers
% total CTB+ cells
Chodl Kcnq5 Chodl Kcnq5
TA SOL
j
Slow motor markers
Positive
Negative
% total CTB+ cells
Sv2a Prkcd Sv2a Prkcd
TA SOL

Table 2 | Enriched Gene Ontology (GO) terms among genes in fast- and slow-firing expression modules

	Voltage-gated K^+ channels	Calmodulin binding	Calcium ion binding	Protein kinase C activity
GO term	GO:0005249	GO:0005516	GO:0005509	GO:0019901
GO term adj *P* value	4.40×10^{-5}	1.50×10^{-4}	6.70×10^{-4}	4.10×10^{-2}
Fast enriched	*Kcnq5, Kcnt2*		*Edil3, Cdh6, Dgkg, Mctp1, Mcc*	*Prkcb*
Slow enriched	*Kcnq3, Kcnc2, Kcnd2*	*Adcy8, Esrrg, Kcnn3, Kcnq3, Unc13c*	*Crtac1, Plch1, Fstl4, Dner*	*Prkcd*

of functionally defined cell populations (akin to performing laser-capture microdissection on an anatomically distinct population of cells). In other words, the individual marker genes that we derive are not the end goal of these experiments but, rather, a means to define the full transcriptome of functionally defined motor neuron populations. To accomplish this, we first demonstrated that IF adult motor neurons express the developmentally defined IF marker *Cpne4* (Fig. 4d,e), whereas other populations of motor neurons (GLUT) do not. This experiment enabled the tentative conclusion that cluster 3 from our transcriptional data corresponds to IF motor neurons labeled by CTB, because *Cpne4* was exclusively expressed in that population using orthogonal methods. However, to conclusively demonstrate this finding, we tested a novel, functionally intriguing marker that we found specifically expressed in cluster 3 of our single-nucleus experiment (*Hcrtr2*). Similarly, this gene was a robust marker of IF motor neurons (87% of IF motor neurons are *Hcrtr2*$^+$) and not substantially expressed in GLUT motor neurons (21% of GLUT motor neurons are *Hcrtr2*$^+$) (Fig. 4d,e). It is intriguing that a specific marker of IF motor neurons, *Hcrtr2*, encodes a membrane-bound hypocretin (orexin) receptor, a gene whose disruption causes muscle weakness and cataplexy in animal models[43].

We next examined whether *Sema3e*$^+$ clusters present in our dataset correspond to the GLUT motor pool. Indeed, we found an increase in proportion of both *Sema3e*$^+$ and *Cdh8*$^+$ cells in GLUT-innervating motor neurons when compared to the IF motor pool (Extended Data Fig. 6a). Overall, our results demonstrate that motor pools in the adult mouse have distinct transcriptional properties that can be resolved by single-nucleus sequencing of α motor neurons. Still, there are far more motor pools (~50)[4] than clusters (12). To explain this discrepancy, we propose that transcriptional differences among adult α motor neurons are more subtle than those that emerge during embryonic development, as is the case in the olfactory system[44], and single-nucleus profiling is only sufficient to delineate more dramatic transcriptional differences. We show that the embryonic marker for GLUT-innervating motor neurons (*Sema3e*) is less specific in the adult mouse, suggesting that future work should seek to use more robust, novel markers (like the ones identified here) to map transcriptional subpopulations onto their peripheral targets. The abundance of specifically expressed genes in each novel population will empower further functional study of the adult motor system.

Fast- and slow-firing α motor neurons have divergent transcriptional signatures

Skeletal muscles innervated by motor neurons are composed of slow (type I), intermediate (type IIa) and fast (type IIx/IIb) twitch fibers, each of which requires different patterns of synaptic input (Fig. 4f)[31]. Likewise, α motor neurons innervating these fibers are divided into slow-firing (SF), fast fatigue-resistant (FR) and fast-fatigable (FF) cell types, each with specific electrophysiological and metabolic properties[33]. Importantly, these groups of α motor neurons have drastically different susceptibilities to degeneration in neuromuscular disorders such as ALS[5,45]. Thus, determining the transcriptional programs that define these classes of motor neurons might provide insight into divergent function and susceptibility to disease[5,31]. Past work has begun to address this question, leading to the discovery of several markers of FF/FR (*Chodl* and *Mmp9*)[5] and SF (*Sv2a*) motor neurons. However, the broader transcriptional differences beyond these few validated markers have thus far remained elusive.

To identify the gene expression modules that underlie differences among SF, FR and FF motor neurons, we segmented all α motor neurons by their mutually exclusive expression of the known markers *Chodl* (fast firing) and *Sv2a* (slow firing)[46]. We identified differentially expressed genes between *Chodl*$^+$ and *Sv2a*$^+$ α motor neurons and then hierarchically clustered cells based on expression of this gene set (Fig. 4g). This analysis was sufficient to segment α motor neurons into three main populations (Fig. 4g). It is clear that fast and slow gene modules are expressed in reciprocal populations of α motor neurons across virtually all motor pools but in different proportions (Extended Data Fig. 6c,d). Notably, hierarchical clustering of cells revealed three main populations of cells, two of which are *Chodl*$^+$ and one that is *Sv2a*$^+$. As *Chodl* is expressed in both FF and FR motor neurons, and *Sv2a* is expressed in SF motor neurons, this raises the possibility that the three populations might, in fact, correspond to FF, FR and SF α motor neurons. We identified novel transcripts to distinguish each population, including a putative marker of FF α motor neurons (*Kcnq5*) and a specific marker of SF motor neurons (*Prkcd*). To confirm these findings, we demonstrated that *Kcnq5* is expressed in a subpopulation of *Chodl*$^+$ (FF/FR) and *Mmp9*$^+$ (FF/FR) α motor neurons (Extended Data Figs. 6e,f and 7a). We also validated that *Prkcd* is expressed in *Sv2a*$^+$ α motor neurons and is excluded from *Mmp9*$^+$ motor neurons (Extended Data Fig. 7b,c).

To validate that the expression of the fast- and slow-firing gene modules that we identified define electrophysiological subtypes of motor neurons, we leveraged unique properties of the soleus (SOL) and tibialis anterior (TA) muscles, which consist of predominantly slow- and fast-twitch fibers, respectively[5,47]. We performed intramuscular CTB injections that label TA- and SOL-innervating motor neurons and measured expression of novel FF and SF marker genes by in situ hybridization (Fig. 4h–j and Extended Data Figs. 6b and 7d,e). In SOL-innervating motor neurons, *Prkcd* was expressed in 69% of cells, whereas *Kcnq5* was expressed in just 29%. This trend was opposite in the TA, which contained 54% *Kcnq5*$^+$ cells and only 28% *Prkcd*$^+$ cells (Extended Data Fig. 7d,e). We observed almost identical patterns of expression for *Prkcd* and *Sv2a*; however, it was clear that, within these motor pools, *Kcnq5* was expressed in only a subpopulation of FF motor neurons. Intriguingly, the proportion of *Kcnq5*$^+$ cells in the TA (54%) is quite close to the proportion of type IIb fibers in that muscle[47]. These data support the conclusion that *Kcnq5* is expressed in FF motor neurons, whereas *Chodl* is more broadly expressed in FF and FR motor neurons—although future electrophysiological characterization will be required to demonstrate this conclusively. In addition, *Prkcd* is a robust and specific marker of SF motor neurons.

Both the FF and SF expression modules contain genes that encode subunits of voltage-gated potassium channels (Table 2). Potassium channel subtypes play a vital role in determining the resting membrane potential and basal firing rate of neurons. The differential expression of potassium channel isoforms suggests a mechanism through which α motor neuron electrophysiological

properties are established[31]. Furthermore, we found that SF neurons specifically express *Prkcd*, which encodes a protein with a fundamental role in determining how cells respond to oxidative stress and DNA damage. In contrast, FF motor neurons do not express *Prkcd* but, instead, express high levels of *Prkcb* (Table 2), which encodes a key regulator of autophagy. Dysregulation of each of these pathways is thought to be fundamental to ALS ontology and progression. Collectively, these data reveal a rich transcriptional basis for the functional diversity of fast- and slow-firing motor neurons.

Discussion

We report here a detailed molecular characterization of the adult mammalian motor system at single-cell resolution. Using a transgenic motor neuron enrichment strategy, we have greatly expanded the transcriptional characterization of these populations and discovered new divisions within the autonomic and somatic motor systems. While we were concluding our studies, an independent group used an orthologous nuclei enrichment and sequencing strategy to provide insight into the heterogeneity of cholinergic neurons in the adult mouse spinal cord[48].

Within the autonomic motor system, we discovered 16 subpopulations of sympathetic visceral motor neurons, including several clusters that localize to the sacral spinal cord. Visceral motor neuron subtypes express entirely different repertoires of neuromodulatory peptides, such as somatostatin, neurotensin and proenkephalin. This suggests an underlying peptidergic logic that governs transmission between visceral motor neurons and their peripheral targets—a long-standing hypothesis that has never been comprehensively demonstrated. Together, our findings inspire the possibility that specific visceral motor neuron populations might someday be selectively targeted with therapies to treat autonomic dysfunction in humans.

Within the somatic motor system, we present novel α and γ motor neuron markers and have identified a new skeletal motor neuron population (γ*), which shares the expected features of the elusive β motor neuron population. Furthermore, we found that transcriptional subpopulations of α motor neurons correspond to previously described, distinct motor pools[37,41]. We propose that other transcriptionally distinct α motor neuron populations in our dataset might similarly correspond to specialized motor pools, and we offer many novel markers to facilitate testing this hypothesis.

Our analysis also reveals gene modules that are selectively expressed in electrophysiologically and metabolically distinct populations of fast- and slow-firing α motor neurons. These differentially expressed genes offer insight into how motor neuron subtypes establish unique biophysical properties that are specifically matched to the properties of their muscle innervation targets[31]. Indeed, our analysis reveals that fast- and slow-firing α motor neurons express a divergent collection of potassium channel subunits that are specifically required to tune the resting membrane potential and firing rate in neurons. These expression profiles might also help suggest approaches to rescue aberrant function in FF motor neurons, which specifically degenerate in ALS[5,33,45,49].

We have identified new markers for motor neuron populations, unlocking unprecedented genetic access to these important cells in the adult spinal cord. Defining the transcriptomes of distinct motor neuron types introduces the possibility of engineering more refined stem cell models and provides a single-cell framework for characterizing their behavior in health and disease.

Online content

Any methods, additional references, Nature Research reporting summaries, source data, extended data, supplementary information, acknowledgements, peer review information; details of author contributions and competing interests; and statements of data and code availability are available at https://doi.org/10.1038/s41593-020-00795-0.

Received: 4 October 2020; Accepted: 23 December 2020;
Published online: 15 February 2021

References

1. Haase, G. et al. GDNF acts through PEA3 to regulate cell body positioning and muscle innervation of specific motor. *Neuron* **35**, 893–905 (2002).
2. Song, M.-R. & Pfaff, S. L. Hox genes: the instructors working at motor pools. *Cell* **123**, 363–365 (2005).
3. Arber, S. Motor circuits in action: specification, connectivity, and function. *Neuron* **74**, 975–989 (2012).
4. Dasen, J. S., Tice, B. C., Brenner-Morton, S. & Jessell, T. M. A hox regulatory network establishes motor neuron pool identity and target-muscle connectivity. *Cell* **123**, 477–491 (2005).
5. Kaplan, A. et al. Neuronal matrix metalloproteinase-9 is a determinant of selective neurodegeneration. *Neuron* **81**, 333–348 (2014).
6. Maniatis, S. et al. Spatiotemporal dynamics of molecular pathology in amyotrophic lateral sclerosis. *Science* **364**, 89–93 (2019).
7. Sathyamurthy, A. et al. Massively parallel single nucleus transcriptional profiling defines spinal cord neurons and their activity during behavior. *Cell Rep.* **22**, 2216–2225 (2018).
8. Sweeney, L. B. et al. Origin and segmental diversity of spinal inhibitory interneurons. *Neuron* **97**, 341–355.e3 (2018).
9. Prigge, J. R. et al. Nuclear double-fluorescent reporter for in vivo and ex vivo analyses of biological transitions in mouse nuclei. *Mamm. Genome* https://doi.org/10.1007/s00335-013-9469-8 (2013).
10. Sunkin, S. M. et al. Allen Brain Atlas: an integrated spatio-temporal portal for exploring the central nervous system. *Nucleic Acids Res.* **41**, D996–D1008 (2013).
11. Burrill, J. D., Moran, L., Goulding, M. D. & Saueressig, H. PAX2 is expressed in multiple spinal cord interneurons, including a population of EN1$^+$ interneurons that require PAX6 for their development. *Development* **124**, 4493–4503 (1997).
12. Espinosa-Medina, I. et al. The sacral autonomic outflow is sympathetic. *Science* **354**, 893–897 (2016).
13. Rosenberg, A. B. et al. Single-cell profiling of the developing mouse brain and spinal cord with split-pool barcoding. *Science* **360**, 176–182 (2018).
14. Thaler, J. P. et al. A postmitotic role for Isl-class LIM homeodomain proteins in the assignment of visceral spinal motor neuron identity. *Neuron* **41**, 337–350 (2004).
15. Dasen, J. S., De Camilli, A., Wang, B., Tucker, P. W. & Jessell, T. M. Hox repertoires for motor neuron diversity and connectivity gated by a single accessory factor, FoxP1. *Cell* **134**, 304–316 (2008).
16. Gilbey, M. P. & Stein, R. D. Characteristics of sympathetic preganglionic neurones in the lumbar spinal cord of the cat. *J. Physiol.* **432**, 427–443 (1991).
17. Gladwell, S. J. & Coote, J. H. Inhibitory and indirect excitatory effects of dopamine on sympathetic preganglionic neurones in the neonatal rat spinal cord in vitro. *Brain Res.* **818**, 397–407 (1999).
18. Yoshimura, M., Polosa, C. & Nishi, S. Slow EPSP and the depolarizing action of noradrenaline on sympathetic preganglionic neurons. *Brain Res.* **414**, 138–142 (1987).
19. de Groat, W. C. et al. The role of neuropeptides in the sacral autonomic reflex pathways of the cat. *J. Auton. Nerv. Syst.* **7**, 339–350 (1983).
20. Parry, L. J., McGuane, J. T., Gehring, H. M., Kostic, I. G. T. & Siebel, A. L. Mechanisms of relaxin action in the reproductive tract: studies in the relaxin-deficient (*Rlx*$^{-/-}$) mouse. *Ann. N. Y. Acad. Sci.* **1041**, 91–103 (2005).
21. Ivell, R., Kotula-Balak, M., Glynn, D., Heng, K. & Anand-Ivell, R. Relaxin family peptides in the male reproductive system—a critical appraisal. *MHR Basic Sci. Reprod. Med.* **17**, 71–84 (2010).
22. Zogovic, B. & Pilowsky, P. M. Intrathecal neurotensin is hypotensive, sympathoinhibitory and enhances the baroreflex in anaesthetized rat. *Br. J. Pharmacol.* **166**, 378–389 (2012).
23. Franz, D. N., Madsen, P. W., Peterson, R. G. & Sangdee, C. Functional roles of monoaminergic pathways to sympathetic preganglionic neurons. *Clin. Exp. Hypertens. A* **4**, 543–562 (1982).
24. Miles, G. B., Hartley, R., Todd, A. J. & Brownstone, R. M. Spinal cholinergic interneurons regulate the excitability of motoneurons during locomotion. *Proc. Natl. Acad. Sci. USA* **104**, 2448–2453 (2007).
25. Zagoraiou, L. et al. A cluster of cholinergic premotor interneurons modulates mouse locomotor activity. *Neuron* **64**, 645–662 (2009).
26. Enjin, A. et al. Identification of novel spinal cholinergic genetic subtypes disclose chodl and Pitx2 as markers for fast motor neurons and partition cells. *J. Comp. Neurol.* **518**, 2284–2304 (2010).
27. Maluenda, J. et al. Mutations in *GLDN*, encoding gliomedin, a critical component of the nodes of Ranvier, are responsible for lethal arthrogryposis. *Am. J. Hum. Genet.* **99**, 928–933 (2016).

28. Stepien, A. E., Tripodi, M. & Arber, S. Monosynaptic rabies virus reveals premotor network organization and synaptic specificity of cholinergic partition cells. *Neuron* **68**, 456–472 (2010).
29. Demireva, E. Y., Shapiro, L. S., Jessell, T. M. & Zampieri, N. Motor neuron position and topographic order imposed by β- and γ-catenin activities. *Cell* **147**, 641–652 (2011).
30. Price, S. R. & Briscoe, J. The generation and diversification of spinal motor neurons: signals and responses. *Mech. Dev.* **121**, 1103–1115 (2004).
31. Muller, D. et al. Dlk1 promotes a fast motor neuron biophysical signature required for peak force execution. *Science* **343**, 1264–1266 (2014).
32. Friese, A. et al. Gamma and alpha motor neurons distinguished by expression of transcription factor Err3. *Proc. Natl Acad. Sci. USA* **106**, 13588–13593 (2009).
33. Stifani, N. Motor neurons and the generation of spinal motor neuron diversity. *Front. Cell. Neurosci.* **8**, 1–22 (2014).
34. Enjin, A. et al. Sensorimotor function is modulated by the serotonin receptor 1d, a novel marker for gamma motor neurons. *Mol. Cell. Neurosci.* **49**, 322–332 (2012).
35. Morisaki, Y. et al. Selective expression of osteopontin in ALS-resistant motor neurons is a critical determinant of late phase neurodegeneration mediated by matrix metalloproteinase-9. *Sci. Rep.* **6**, 27354 (2016).
36. Barker, D., Emonet-Dénand, F., Harker, D. W., Jami, L. & Laporte, Y. Types of intra- and extrafusal muscle fibre innervated by dynamic skeleto-fusimotor axons in cat peroneus brevis and tenuissimus muscles, as determined by the glycogen-depletion method. *J. Physiol.* **266**, 713–726 (1977).
37. Mendelsohn, A. I., Dasen, J. S. & Jessell, T. M. Divergent hox coding and evasion of retinoid signaling specifies motor neurons innervating digit muscles. *Neuron* **93**, 792–805 (2017).
38. Machado, T. A., Pnevmatikakis, E., Paninski, L., Jessell, T. M. & Miri, A. Primacy of flexor locomotor pattern revealed by ancestral reversion of motor neuron identity. *Cell* **162**, 338–350 (2015).
39. Landmesser, L. T. The generation of neuromuscular specificity. *Annu. Rev. Neurosci.* **3**, 279–302 (1980).
40. Fukuhara, K. et al. Specificity of monosynaptic sensory-motor connections imposed by repellent Sema3E-PlexinD1 signaling. *Cell Rep.* **5**, 748–758 (2013).
41. Pecho-Vrieseling, E., Sigrist, M., Yoshida, Y., Jessell, T. M. & Arber, S. Specificity of sensory-motor connections encoded by Sema3e-Plxnd1 recognition. *Nature* **459**, 842–846 (2009).
42. Sürmeli, G., Akay, T., Ippolito, G. C., Tucker, P. W. & Jessell, T. M. Patterns of spinal sensory-motor connectivity prescribed by a dorsoventral positional template. *Cell* **147**, 653–665 (2011).
43. Lin, L. et al. The sleep disorder canine narcolepsy is caused by a mutation in the hypocretin (orexin) receptor 2 gene. *Cell* **98**, 365–376 (1999).
44. Li, H. et al. Classifying *Drosophila* olfactory projection neuron subtypes by single-cell RNA sequencing. *Cell* **171**, 1206–1220 (2017).
45. Nijssen, J., Comley, L. H. & Hedlund, E. Motor neuron vulnerability and resistance in amyotrophic lateral sclerosis. *Acta Neuropathol.* **133**, 863–885 (2017).
46. Chakkalakal, J. V., Nishimune, H., Ruas, J. L., Spiegelman, B. M. & Sanes, J. R. Retrograde influence of muscle fibers on their innervation revealed by a novel marker for slow motoneurons. *Development* **137**, 3489–3499 (2010).
47. Kammoun, M., Cassar-Malek, I., Meunier, B. & Picard, B. A simplified immunohistochemical classification of skeletal muscle fibres in mouse. *Eur. J. Histochem.* **58**, 2254 (2014).
48. Alkaslasi, M. R. et al. Single nucleus RNA-sequencing defines unexpected diversity of cholinergic neuron types in the adult mouse spinal cord. Preprint at *bioRxiv* https://doi.org/10.1101/2020.07.16.193292 (2020).
49. Taylor, J. P., Brown, R. H. J. & Cleveland, D. W. Decoding ALS: from genes to mechanism. *Nature* **539**, 197–206 (2016).
50. Stuart, T. et al. Comprehensive integration of single-cell data. *Cell* **177**, 1888–1902 (2019).

Methods

Data reporting. No statistical methods were used to predetermine sample size, but our sample sizes (such as minimum cluster size) are similar to those reported in previous publications[7,13,50]. No randomization was used in assigning experimental conditions to animals. All quantification of microscopy images was performed blinded. CTB experiments were included in analysis if, under blinded conditions, it was determined that CTB-labeled cells were easily distinguishable from background staining (for example, successful retrograde labeling occurred). Additional information can be found in the Life Sciences Reporting Summary.

Statistics. For in situ hybridization quantifications, one-way analysis of variance (ANOVA) tests with Sidak and Tukey post tests were used to determine statistical significance of differences among specific comparisons (Sidak) or all conditions (Tukey). For single-cell analysis, all pseudo-bulk differential expression was calculated using the Wilcoxon rank sum test and adjusted for multiple comparisons (Bonferroni method), implemented, by default, in Seurat[50]. These tests did not require assumptions of normally distributed data.

Mouse crosses. ChaT-IRES-Cre (Chat-CRE/Chat-CRE) mice were purchased from JAX (stock no. 006410m B6; 129S6-*Chat*$^{tm2(cre)Lowl}$/J) and crossed with ROSA$^{nT\text{-}nG}$/ROSA$^{nT\text{-}nG}$ (stock no. 023035 B6; 129S6-*Gt(ROSA)26Sor*$^{tm1(CAG\text{-}tdTomato^*,\text{-}EGFP^*)Ees}$/J). F_1 heterozygous reporter mice were aged to P100–150 and then sacrificed for subsequent sequencing experiments. All in situ hybridization was performed using wild-type male and female P100–150 B6 mice purchased from JAX (stock no. 000664). Mice were housed at ~55% humidity, 25 °C, on a 12:12-h light/dark cycle. Humane experiments were performed with ethical oversight by the Stanford Administrative Panel on Laboratory Testing (protocol no. 30643).

Mouse nuclei collection. Four to eight mice in five independent experiments were euthanized with CO_2 and decapitated caudal to the brain stem. Their spinal columns were severed just caudal to the sacral spinal cord and rapidly cut out as described[7]. Briefly, a blunt 18-gauge syringe containing ice-cold PBS was inserted into the caudal end of the spinal cord and used for rapid hydraulic extrusion of the entire, intact cord. Two spinal cords at a time were homogenized with a Dounce Homogenizer in 2 ml of nuclei extraction buffer (Supplementary Table 4a). Spinal cords were homogenized with ten strokes of Pestle A, followed by five strokes of Pestle B. The entire homogenate was transferred to a 25-ml, round-bottom plastic ultracentrifuge tube, and 8 ml of nuclei spin buffer 1 (Supplementary Table 4a) was added. Five milliliters of nuclei spin buffer 2 (Supplementary Table 4a) was layered gently underneath the homogenate, and the gradient was spun for 15 min at 4,000*g* in a 4 °C benchtop swinging bucket centrifuge (Beckman, 5810R). The supernatant was rapidly discarded, and the nuclei were gently resuspended in 5 ml of nuclei spin buffer 1. Five milliliters of nuclei spin buffer 3 was gently layered underneath, and the resulting gradient was spun for 15 min at 4,000*g* at 4 °C. The supernatant was rapidly discarded, and the pellet was resuspended in 400 µl of nuclei FACS buffer. Next, 0.5 µl of DAPI was added to enable doublet discrimination on the sorter.

Fluorescence-activated nuclei sorting. Fluorescence-activated nuclei sorting was performed on a BD Biosciences FACSAria II flow cytometer. Briefly, after calibration of the FACS machine or power-up of the flow cytometer, single nuclei were gated using forward scatter, side scatter and DAPI measurements to ensure that doublets were gated out. After this initial gating, EGFP$^+$/tdTomato$^-$ nuclei were identified using a two-dimensional scatterplot. These nuclei stood out from the main population, enabling double gating. To ensure that our samples would contain both cholinergic and non-cholinergic nuclei, we then sorted ~10,000–15,000 EGFP$^+$/tdTomato$^-$ nuclei and 20,000–25,000 EGFP$^-$/tdTomato$^+$ nuclei into 400 µl of 10× loading buffer (Supplementary Table 4a). After sorting was completed, this nuclei mixture was spun at 300*g* for 5 min and resuspended in 10× loading buffer according to 10× loading criteria for the precise number of nuclei sorted—a number that varied.

Droplet-based snRNA-seq. For droplet-based snRNA-seq, libraries were prepared using the Chromium Single Cell 3′ Reagent Kit v3 according to the manufacturer's protocol (10x Genomics). The generated snRNA-seq libraries were sequenced using NextSeq 500/550 High Output v2 kits (150 cycles) to an average read depth of ~500,000 reads per cell.

Mouse CNS in situ hybridization. Mice were humanely euthanized using CO_2 for 5 min before decapitation. The spinal cord was rapidly hydraulically extruded, as above, and briefly dried. For longitudinal sections, the spinal cord was placed into a plastic freezing mold and frozen briefly on dry ice, before adding O.C.T. compound freezing media (Tissue-Tek) to ensure that the spinal cord was frozen completely flat to the mold. For transverse sections, spinal cords were cut into three segments: roughly lumbosacral, thoracic and cervical. Sections were mounted and cut to a thickness of 20 µm using a Leica CM3050 S Cryostat. Sections were processed immediately or stored for 1–2 weeks at −80 °C.

Sections were processed for RNAScope v2 (ACD Biosciences) according to manufacturer instructions for fresh frozen tissue. All in situ hybridization probes used are listed in Supplementary Table 4b. Briefly, tissue sections were fixed with 4% paraformaldehyde (PFA) at 4 °C and subsequently dehydrated with 5 min each of 50% EtOH, 70% EtOH and, finally, 100% EtOH. Samples were dried, and a hydrophobic barrier was drawn around each section. Samples were then incubated with Protease IV (ACD Biosciences) for 15 min at room temperature before removing and washing in 1× PBS. Before staining, probes were equilibrated to 40 °C for 10 min and then cooled to room temperature. Mixtures of probes in channels 1–3 were diluted and then incubated on samples for 2 h in a humidified 40° hybridization oven. Samples were washed twice in PBS and then incubated in the hybridization oven at 40° with Amp-1-FL, Amp-2-FL, Amp-3-FL and Amp-4-FL for 30, 15, 30 and 15 min, respectively (with 2× washes in between each incubation). Samples were then washed twice, briefly dried and mounted with DAPI-containing VECTASHIELD mounting media (Vector Laboratories, H-1200-10). Subsequent imaging was performed using a Zeiss LSM 710 confocal microscope. Image analysis and background correction were performed in ImageJ.

Analysis of snRNA-seq data. Counts per gene were generated by aligning reads to the mm10 genome (Mus_musculus.GRCm38—NCBI: GCA_000001635.2) using CellRanger software (v3.0.0) (10x Genomics) running on the Sherlock Stanford Computing Cluster. To account for unspliced nuclear transcripts, reads mapping to pre-mRNA were counted. After this, the CellRanger aggr pipeline was used to aggregate all libraries and normalize the read depth between libraries before data merging (with the default parameters) to generate a gene count matrix. We then used the cell detection method employed by CellRanger to exclude doublets and empty droplets (10x Genomics).

Normalization, clustering and subtype annotation. Most subsequent analysis was performed using the Seurat R Package[50] (https://satijalab.org, v3.0). All 43,890 transcriptomes were normalized for read depth with the CellRanger aggr function and then loaded into Seurat. The nuclei were batch corrected using the Seurat *Integrate* function as previously described[50], which enables cells from different experiments to be projected into the same high- and low-dimensional spaces. Principal component analysis was performed on the whole dataset, and the top 15 components were used to generate a uniform manifold approximation and projection (UMAP). The same principal components were used to perform graph-based clustering via the *FindClusters* function, which identified 39 total clusters, several of which were manually identified as doublet clusters and removed. To annotate remaining clusters, a manually curated list of markers for major cell types was assembled from the literature, including excitatory interneurons, inhibitory interneurons, cholinergic neurons, oligodendrocytes, endothelial cells, astrocytes and microglia. Average expression of these marker genes was calculated using Seurat (*AverageExpression*). Clusters that were positive for these marker genes were annotated by cell type (for example, *Aqp4*$^+$ clusters were classified as astrocytes).

To identify specific marker genes for each neuronal subtype, differential gene expression analysis was performed using the Seurat *FindAllMarkers* function, which leverages Wilcoxon rank sum test differential expression testing. Briefly, differentially expressed genes were identified for each subtype with respect to all remaining cells. Each subtype was downsampled to 250 cells to compensate for stoichiometric biases. A false discovery rate (FDR)-corrected P value threshold was set at $P < 0.01$, and only markers with a $\log_2$ fold change (FC) > 0.5 were included in subsequent analysis. To find robust markers, lists of differentially expressed marker genes were rank order based on the average expression level in all cells not included in the subtype of interest (low background expression yields high rank). Even though this occasionally resulted in the prioritization of markers that are not ubiquitously expressed in the subtype of interest, we determined that this method empirically produces robust markers and viewed the loss of signal in some cells as a likely result of a high dropout rate for single-nucleus sequencing. However, only genes detected in at least 25% of the cells within the given identity class were considered as candidate subtype markers. Skeletal and visceral motor neurons, as well as cholinergic interneurons, were each separately subsetted, subclustered and UMAP projected. Differential expression analysis was performed on clusters within each population, as above and explained in the main text.

To determine batch-to-batch variability and reproducibility of effects, all levels of clustering were plotted as UMAPs for each replicate, along with the age, sex and number of mice that were pooled per replicate (Extended Data Fig. 8). This analysis demonstrated that cluster identity was largely invariant to sex, age and number of mice pooled.

Retrograde labeling. Motor neurons innervating the TA, SOL or IF were retrogradely labeled by contralateral intramuscular injection of CTB subunit conjugated to Alexa 488. Adult mice were deeply anesthetized with 2–3% isoflurane mixed with oxygen. To access the TA and SOL muscles, a small incision was made on the front of one hindlimb (TA) and on the lateral side of the contralateral hindlimb (SOL). For IF muscle injections, CTB solution was directly injected into the footpad. Injections were performed with a 10-µl Hamilton syringe equipped with a 33-gauge needle. For all, muscles were injected at three sites with 0.5 µl of 0.5-1% CTB-488 solution. After each injection, the wound site was closed with 7-mm Reflex clips. Spinal cords (and injected muscles) were harvested 5 d

after injection. For the isolation, muscles were fixed for 20 min in 4% PFA at room temperature. They were washed in PBS, cryopreserved overnight in 30% sucrose and embedded in O.C.T. compound. For the SOL and TA, longitudinal muscle sections were cut at 30 µm on the cryostat. Sections were immunostained with rabbit anti-CTB (Abcam) and bungarotoxin conjugated to CF55 (Biotium). Muscles were analyzed by microscopy to confirm the specificity of CTB labeling.

Tissue preparation. Mice were transcardially perfused with PBS, and spinal cords were removed by hydraulic extrusion. Spinal cords were fixed in 4% PFA overnight at 4 °C. The next day, tissues were washed with PBS before overnight cryoprotection in 30% sucrose. Tissues were embedded in O.C.T. compound, and 20-µm longitudinal sections were acquired on a Leica CM3050S cryostat.

Combined in situ hybridization and immunohistochemistry. Cryosections were rinsed in PBS and baked at 60 °C for 45 min. Slides were then fixed in 4% PFA for 1 h at room temperature. Ethanol dehydration was then performed with 50%, 70%, 100% and 100% ethanol for 5 min each. After air drying, sections were treated with RNAScope hydrogen peroxide for 10 min, followed by antigen retrieval at 95 °C in RNAScope Target Retrieval Buffer. Slides were then baked at 60 °C for 45 min. The remaining steps of the in situ hybridization procedure were performed using the RNAScope Multiplex Fluorescent Reagent Kit v2 according to manufacturer guidelines. Upon completion of the in situ hybridization, CTB immunostaining was performed. Briefly, spinal cord sections were blocked in PBS containing 0.2% Triton-X and 10% donkey serum (Jackson ImmunoResearch). Rabbit anti-CTB (ab34992, Abcam) diluted at 1:8,000 in PBS containing 0.2% Triton-X was incubated overnight at 4 °C. The next day, secondary antibody labeling was performed with donkey anti-rabbit Alexa 488 (Invitrogen).

Image analysis. All sections with CTB retrograde labeling were imaged on a confocal microscope (Leica SP8, Leica Biosystems). ×10 tile scans were acquired at high resolution (2,048 × 2,048) with a z-step size of 2.5 µm using LAS Navigator. Maximum intensity images were generated from merged tile scans (LAS X Software, Leica Biosystems). To prevent counting false-positive motor neurons that were artifactually labeled with CTB leakage, cells with high levels of CTB backfill were uniformly identified in each sample through thresholding. All CTB^+ motor neurons were then scored for the presence or absence of a particular RNAScope probe set.

Visceral motor neuron spatial localization. We determined where cells within each visceral motor neuron subcluster localize along this axis by the following method. Briefly, a list of approximately 100 genes that localize to the intermediolateral cell column (iMLC) was compiled from the Allen Spinal Cord Atlas[10] (Supplementary Table 4c). Among these genes, we identified 29 marker genes differentially expressed in at least one visceral motor neuron subcluster. Differentially expressed genes among visceral clusters were identified as above. We then counted the number of iMLC cells that were positive for each gene in all available adult spinal cord sections in the Allen Spinal Cord Atlas and noted the relative position of each positive cell along the rostral–caudal spinal cord axis. For each marker gene, we divided the number of positive cells at each rostral–caudal section by the average positive cell count for that gene across all sections. We then normalized this cell density by the maximum number of cells in any section that were positive for that gene, to generate a normalized cell count representing the relative enrichment of positive cells in different sections of the spinal cord. Owing to the sparsity of the data, we fit a polynomial function (order = 8) to the normalized count, producing 29 independent polynomial functions (gene densities) that reflect the density of cells expressing each gene over the adult mouse spinal cord. We then estimated the positional density of each scRNA-seq visceral motor neuron cluster as the weighted average of the gene densities for which the gene is differentially expressed in the cluster. The averaging weights were calculated as the $\log_2$ FC of the gene expression level with a given cluster with respect to the mean expression of the gene across all clusters. This generates an estimated positional density for each cluster along the rostral–caudal spinal cord spatial atlas as reported.

If the $\log_2$ FC was > 0 and the FDR-adjusted P value was < 0.01, we considered a cluster enriched for expression of that gene.

Visceral motor neuron spatial validation by in situ hybridization. Spinal cords from wild-type mice were rapidly hydraulically extruded and cut into six uniform pieces, spanning from sacral to upper thoracic spinal cord, and frozen in cryopreservant. Four sequential cryostat sections were cut at 20 µm every 600 µm along the rostral–caudal axis to fully sample the thoracic and sacral autonomic columns. All subsequent tissue processing for RNAScope v2 (ACD Biosciences) was performed according to manufacturer instructions for fresh frozen tissue.

Background subtraction was performed on each channel of all images. For each image, masks of all cholinergic cells were made using the ChAT channel. To make the masks, a pixel value threshold and size cutoff were applied to remove noise, and the resulting images were converted into binary form. Using the binary images, masks corresponding to non-visceral motor neuron cells were manually removed, and, occasionally, visceral motor neuron masks were manually split. Images without visceral motor neurons were not processed.

For each visceral motor neuron mask, mean and maximum pixel values were obtained from the non-ChAT channels, which contain RNA scope data from the genes of interest (*Rxfp1*, *Fbn2*, *Nts*, *Creb5*, *Piezo2*, *Cdh8* and *Cpne4*). This was done by redirecting each binary image to the corresponding image/channel and analyzing particles. For each gene of interest, a threshold was set on the mean and maximum pixel values such that visceral motor neurons surpassing the threshold were counted as expressing the gene of interest. The total number of visceral motor neurons, the number of visceral motor neurons expressing the gene of interest and the percentage of visceral motor neurons expressing the gene of interest were plotted as a function of distance along the rostral–caudal axis. The analysis was performed by a researcher who was blinded to the genes that were probed for.

Accession codes. All raw and processed sequencing data have been deposited in the Gene Expression Omnibus under accession number GSE161621.

Reporting Summary. Further information on research design is available in the Nature Research Reporting Summary linked to this article.

Data availability

All sequencing data are available in raw and processed forms from the National Center of Biotechnology Information's Gene Expression Omnibus (accession no. GSE161621). An interactive web portal for exploring the dataset is available at http://www.spinalcordatlas.org.

Code availability

All custom code used to analyze data and generate figures is available in the form of a Jupyter Notebook at https://github.com/neurojacob/blum_et_al_2021.

Acknowledgements

This work was supported by National Institutes of Health (NIH) grants R35NS097263 (to A.D.G.) and R01NS083998 (to J.A.K.), the Robert Packard Center for ALS Research at Johns Hopkins (to A.D.G.), the Blavatnik Family Foundation (to J.A.B.) and the Brain Rejuvenation Project of the Wu Tsai Neurosciences Institute. Sorting was performed on an instrument in the Shared FACS Facility obtained using NIH S10 Shared Instrument Grant S10RR025518-01. Portions of Figs. 1d and 2b were generated using objects from BioRender.com.

Author contributions

J.A.B. and A.D.G. designed the experiments and wrote the paper. All authors reviewed and edited the manuscript. J.A.B. performed experiments and computational analysis of the data. S.K. and J.L.S. helped plan and perform experiments and analyze data. L.N. helped with mouse husbandry. K.A.G., A.K., P.T.H. and O.G. helped perform experiments. J.A.K. and W.J.G. helped analyze data and provided advice on designing experiments.

Competing interests

A.D.G. has served as a consultant for Aquinnah Pharmaceuticals, Prevail Therapeutics and Third Rock Ventures and is a scientific founder of Maze Therapeutics. W.J.G. has affiliations with 10x Genomics (consultant), Guardant Health (consultant) and Protillion Biosciences (co-founder and consultant). J.A.B. has served as a consultant for Maze Therapeutics.

Additional information

Extended data is available for this paper at https://doi.org/10.1038/s41593-020-00795-0.

Supplementary information The online version contains supplementary material available at https://doi.org/10.1038/s41593-020-00795-0.

Correspondence and requests for materials should be addressed to A.D.G.

Peer review information *Nature Neuroscience* thanks Alain Chédotal and the other, anonymous, reviewer(s) for their contribution to the peer review of this work.

Reprints and permissions information is available at www.nature.com/reprints.

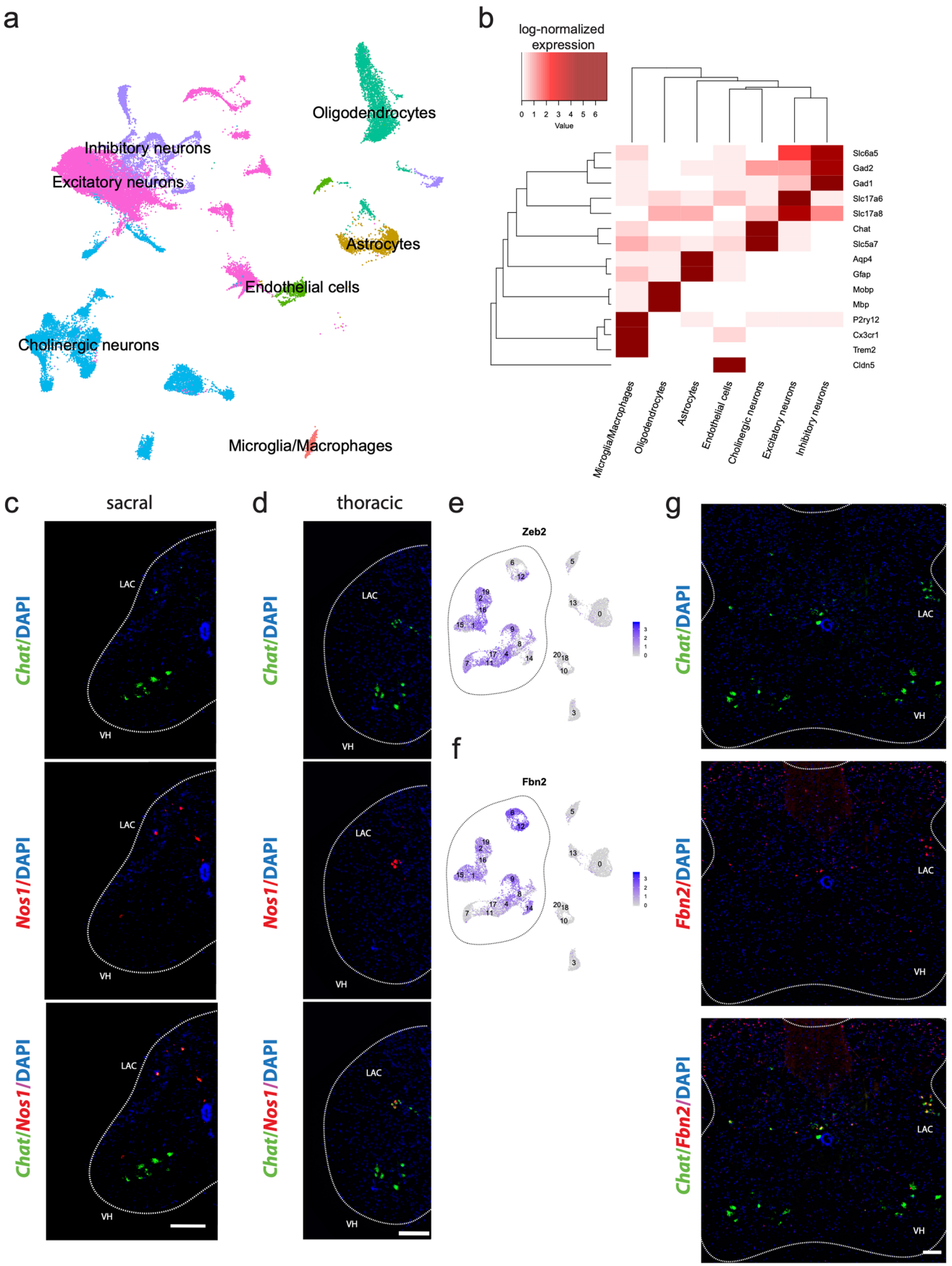

Extended Data Fig. 1 | See next page for caption.

Extended Data Fig. 1 | Single-nucleus transcriptional analysis of the adult mouse spinal cord reveals canonical cell types. a, Canonical cell class labels, visualized on UMAP. **b**, Average log-normalized marker gene expression across canonical cell classes. **c-d**, Representative *in situ* hybridization against *Chat/Nos1* in transverse sacral (**c**) and thoracic (**d**) spinal cord hemi-sections. n = 3 biologically independent animals. **e-f**, Average log-normalized expression of *Zeb2* (**e**) and *Fbn2* (**f**) across all cholinergic clusters (labeled), overlaid on UMAP. Dotted line surrounds clusters corresponding to visceral motor neurons. **g**, Representative *in situ* hybridization against *Chat/Fbn2* in transverse thoracic spinal cord hemi-section. n = 3 biologically independent animals. Scale bars=200 μm (**c**-**d**) and 100 μm (**g**). LAC = lateral autonomic column (**c**,**d**), VH = ventral horn (**c**,**d**).

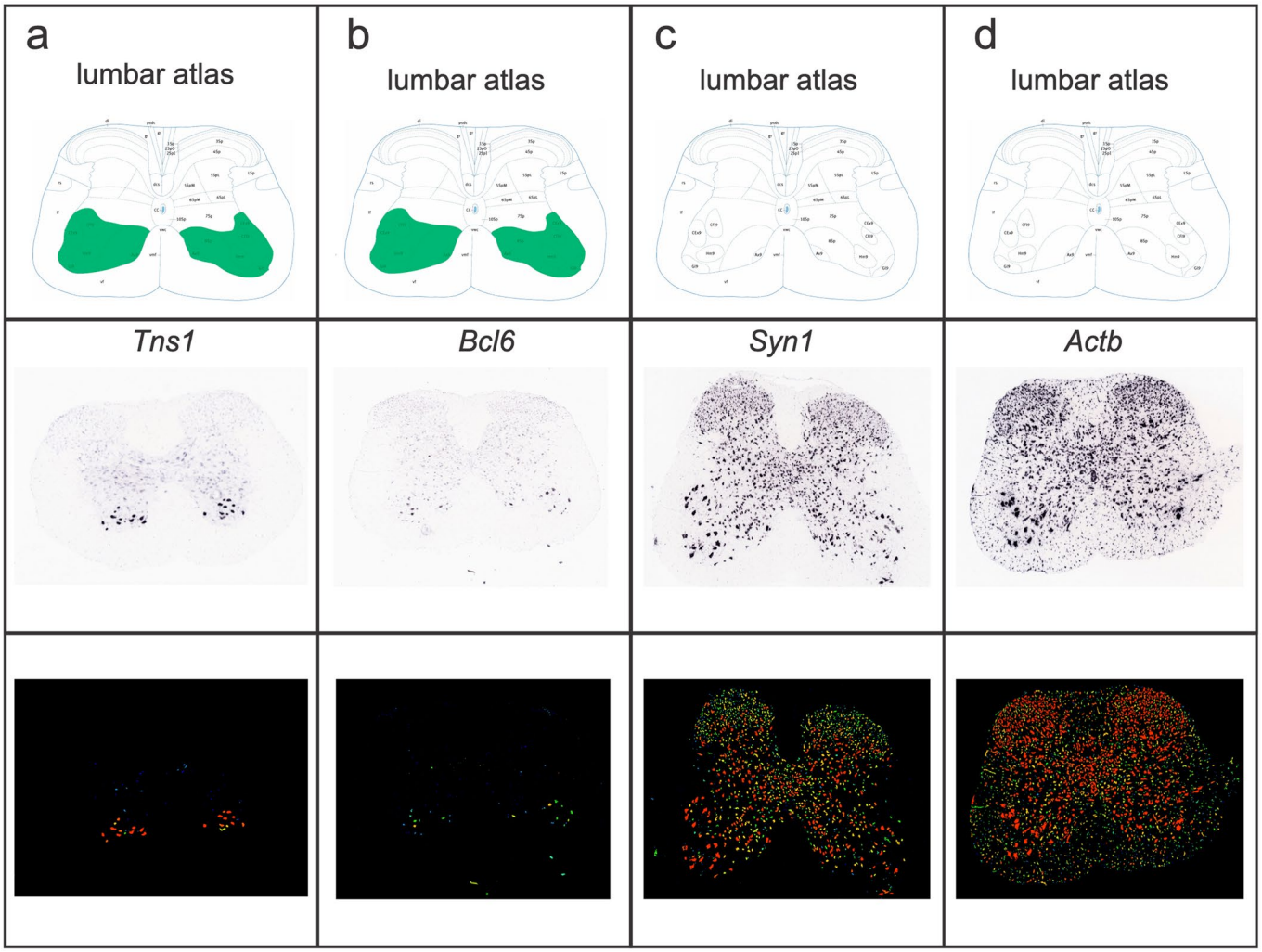

Extended Data Fig. 2 | Novel markers of skeletal motor neurons confirmed by Allen Spinal Cord Atlas in situ hybridizations. a-d, Transverse schematic illustrating expected positions of skeletal motor neurons in ventral horn (VH, green) in lumbar spinal cord. Second row—corresponding *in situ* hybridization against *Tns1* (**a**), *Bcl6* (**b**), *Syn1* (**c**), and *Actb* (**d**). Third row—expression mask shows relative enrichment of *Tns1* and *Bcl6* in small and large cell bodies in the VH.

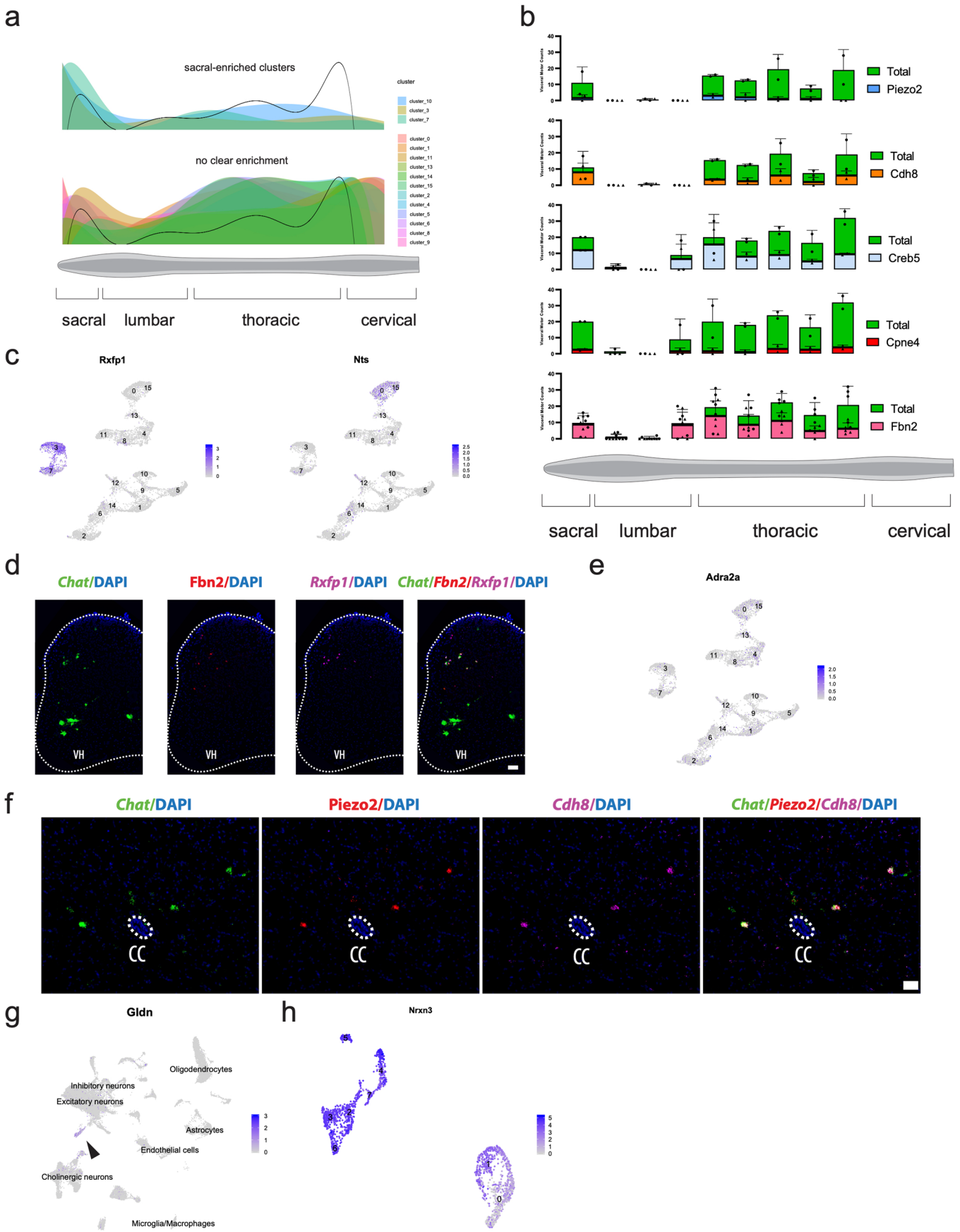

Extended Data Fig. 3 | See next page for caption.

Extended Data Fig. 3 | Visceral motor neuron populations express selective repertoires of neuropeptides and are spatially distinct. a, Estimated relative density of visceral motor neurons along the rostral-caudal axis of the spinal cord based on Allen Spinal Cord Atlas[10]. Density functions are combined density estimates of marker genes for each cluster (see Methods). Clusters were grouped according to shape of density function, with clusters 3,7, and 10 clearly enriched in the sacral spinal cord. **b**, Validation of visceral spatial modeling from (**a**) via high-resolution *in situ* hybridization for *Chat* and visceral cluster markers (*Piezo2, Cdh8, Creb5, Cpne4, Fbn2*). Plots show number of motor neurons counted in the autonomic column, added across three counted slides in each region. Individual data points for total visceral motor neurons shown with filled circles, while marker gene-positive cell numbers shown with filled triangles. n = 2 (*Piezo2, Cdh8, Creb5, Cpne4)* or 5 (*Fbn2)* biologically independent replicates. Error bars are SEM. **c**, Average log-normalized expression of *Rxfp1* and *Nts* across all visceral motor neuron clusters (labeled), overlaid on UMAP. **d**, Representative *in situ* hybridization against *Chat/Fbn2/Rxfp1* in transverse sacral spinal cord shows coexpression in the autonomic column but not in the ventral horn (VH). n = 3 biologically independent animals. Scale bar=100 μm. **e**, Average log-normalized expression of *Adra2a* across all visceral clusters (labeled) shows that sporadic expression exists across populations, overlaid on UMAP. **f**, Representative *in situ* hybridization against *Chat/Piezo2/Cdh8* in cholinergic cells around the central canal (CC). Scale bar=50 μm. n = 2 biologically independent animals. **g**, Average log-normalized expression of *Gldn* across all cells in spinal cord shows clear enrichment in partition cell cluster (arrowhead), overlaid on UMAP. **h**, Average log-normalized expression of *Nrxn3* across cholinergic interneurons shows that *Nrxn3* expression is limited to half of partition cells (arrowhead), overlaid on UMAP.

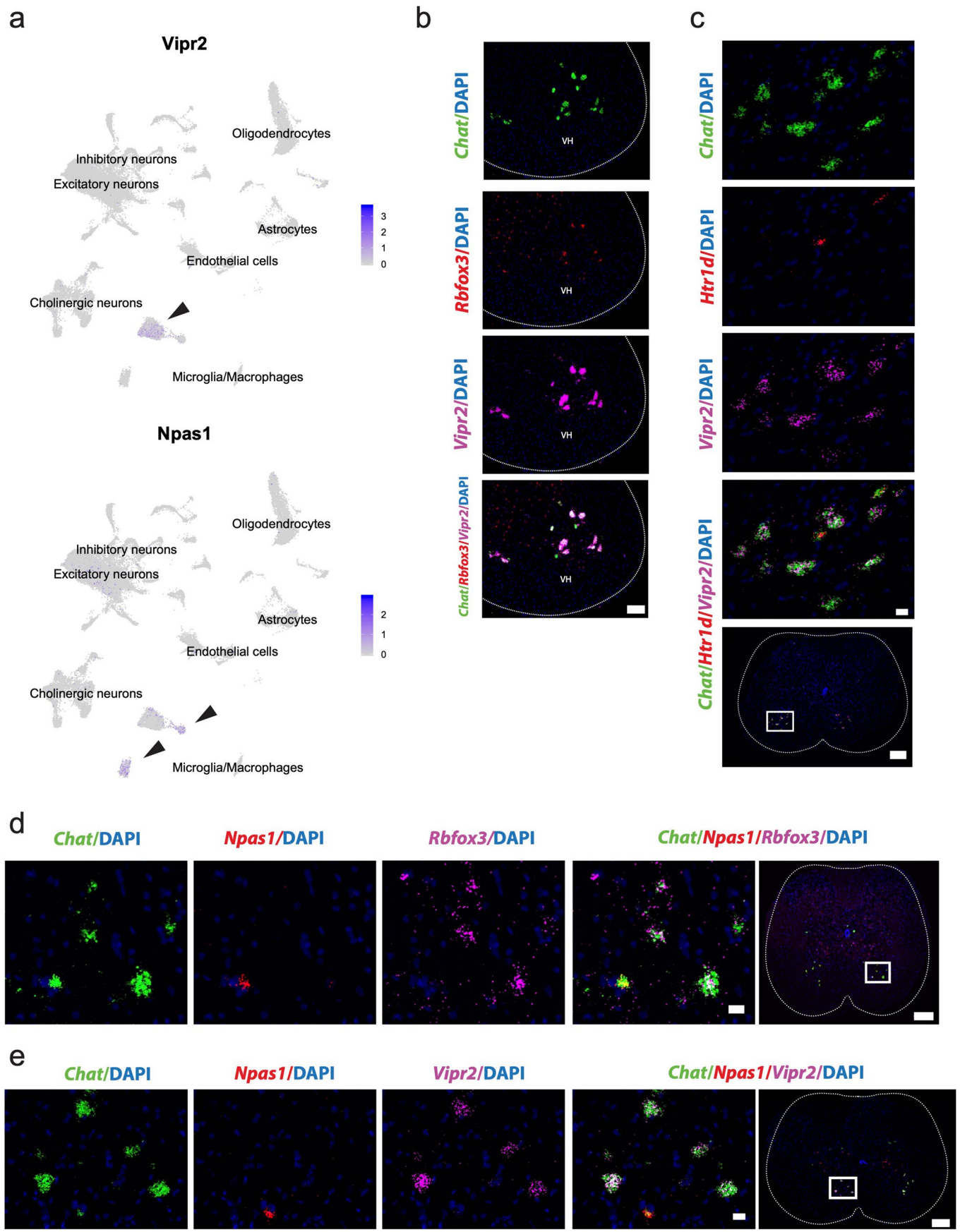

Extended Data Fig. 4 | See next page for caption.

Extended Data Fig. 4 | Vipr2 and Npas1 are novel, robust, and specific markers of α and γ motor neurons in the spinal cord. a, Average expression of *Vipr2* and *Npas1* across all spinal cord cell populations (labeled), overlaid on UMAP. Arrow points to α and γ motor neuron clusters, respectively. **b**, Representative *in situ* hybridization against *Chat/Rbfox3/Vipr2* in transverse spinal cord shows coexpression in the ventral horn (VH). n = 4 biologically independent animals. Scale bar=100 μm. **c**, Representative *in situ* hybridization against *Chat/Htr1d/Vipr2* in transverse spinal cord shows mutual exclusion. Scale bar=50 μm (inset) and 200 μm (overview). n = 4 biologically independent animals. **d**, Representative *in situ* hybridization against *Chat/Npas1/Rbfox3* in transverse spinal cord shows mutual exclusion of *Rbfox3* and *Npas1* in *Chat* + cells. n = 5 biologically independent animals. Scale bar=20 μm (inset) and 200 μm (overview). **e**, Representative *in situ* hybridization against *Chat/Npas1/Vipr2* in transverse spinal cord shows mutual exclusion of novel markers *Vipr2* and *Npas1* in *Chat* + cells. n = 4 biologically independent animals. Scale bar=20 μm (inset) and 200 μm (overview).

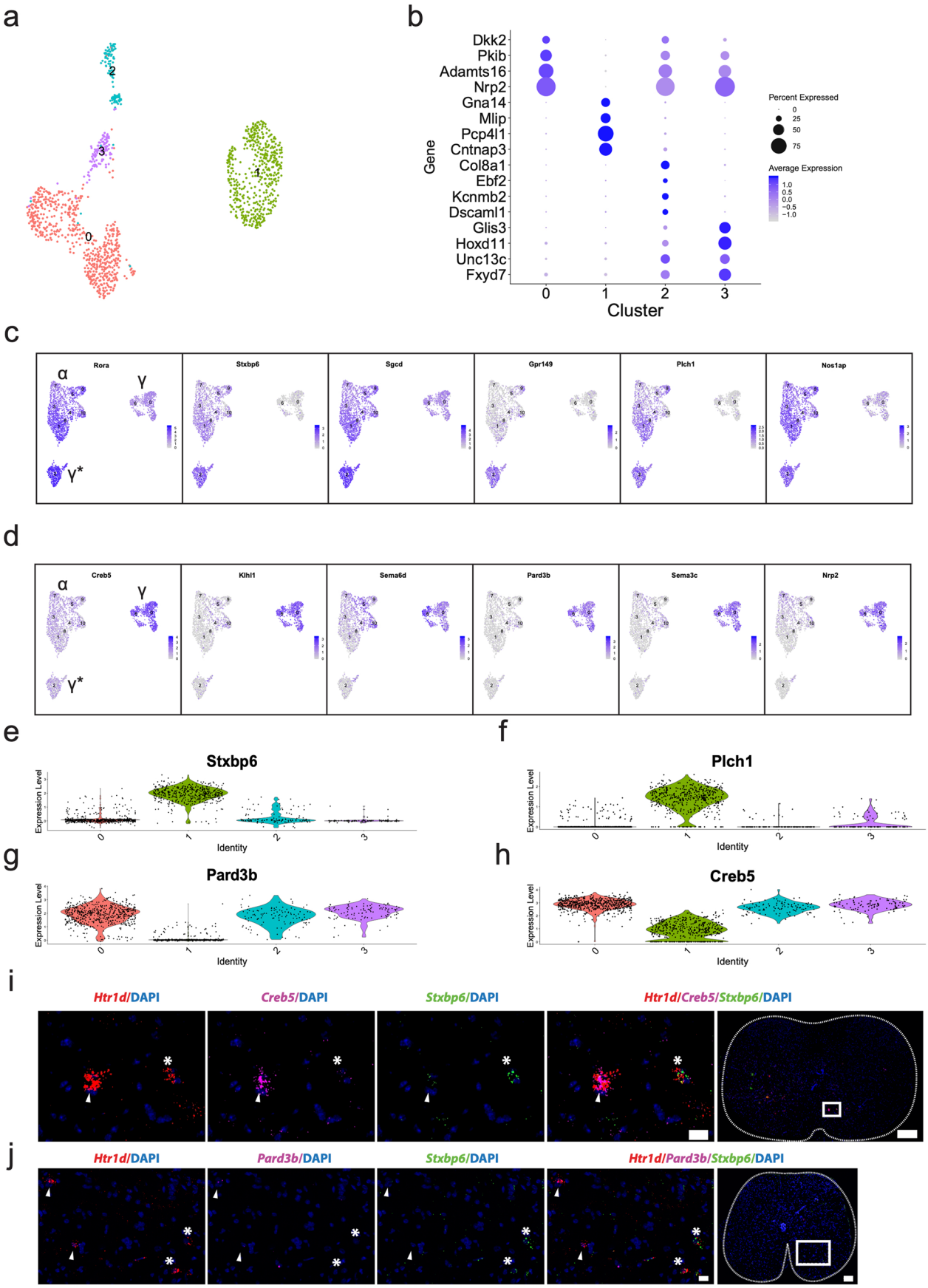

Extended Data Fig. 5 | See next page for caption.

Extended Data Fig. 5 | Discovery of a fundamental transcriptional bifurcation among γ motor neurons. a, UMAP with 3 subclustered γ motor neurons populations. **b**, Novel marker gene expression across γ motor neuron subpopulations. Dot size is proportional to the percent of each cluster expressing the marker gene, while blue color intensity is correlated with expression level. **c**, Average log-normalized expression of genes enriched in γ* motor neurons over γ overlaid on UMAP. α, γ, and γ* populations are labeled. **d**, Average log-normalized expression of genes enriched in γ motor neurons over γ* overlaid on UMAP. α, γ, and γ* populations are labeled. **e-h**, Average expression of novel γ markers *Stxbp6* (**e**) and *Plch1* (**f**), as well as novel γ* markers *Pard3b* (**g**) and *Creb5* (**h**) by cluster. **i**, Representative *in situ* hybridization against *Htr1d/Creb5/Stxbp6* in transverse spinal cord shows mutual exclusion of novel markers *Creb5* and *Stxbp6* in *Htr1d* + cells. n = 4 biologically independent animals. Scale bar=20 μm (inset) and 200 μm (overview). **j**, Representative *in situ* hybridization against *Htr1d/Pard3b/Stxbp6* in transverse spinal cord shows mutual exclusion of novel markers *Pard3b* and *Stxbp6* in *Htr1d* + cells. Arrowheads label canonical γ motor neurons and *labels γ*. n = 5 biologically independent animals. Scale bar=20 μm (inset) and 100 μm (overview). Differentially expressed genes determined by Wilcoxon rank sum test implementation in Seurat and adjusted for multiple comparisons (Bonferroni method) (p_adj<0.01, log2-fold change >0.5).

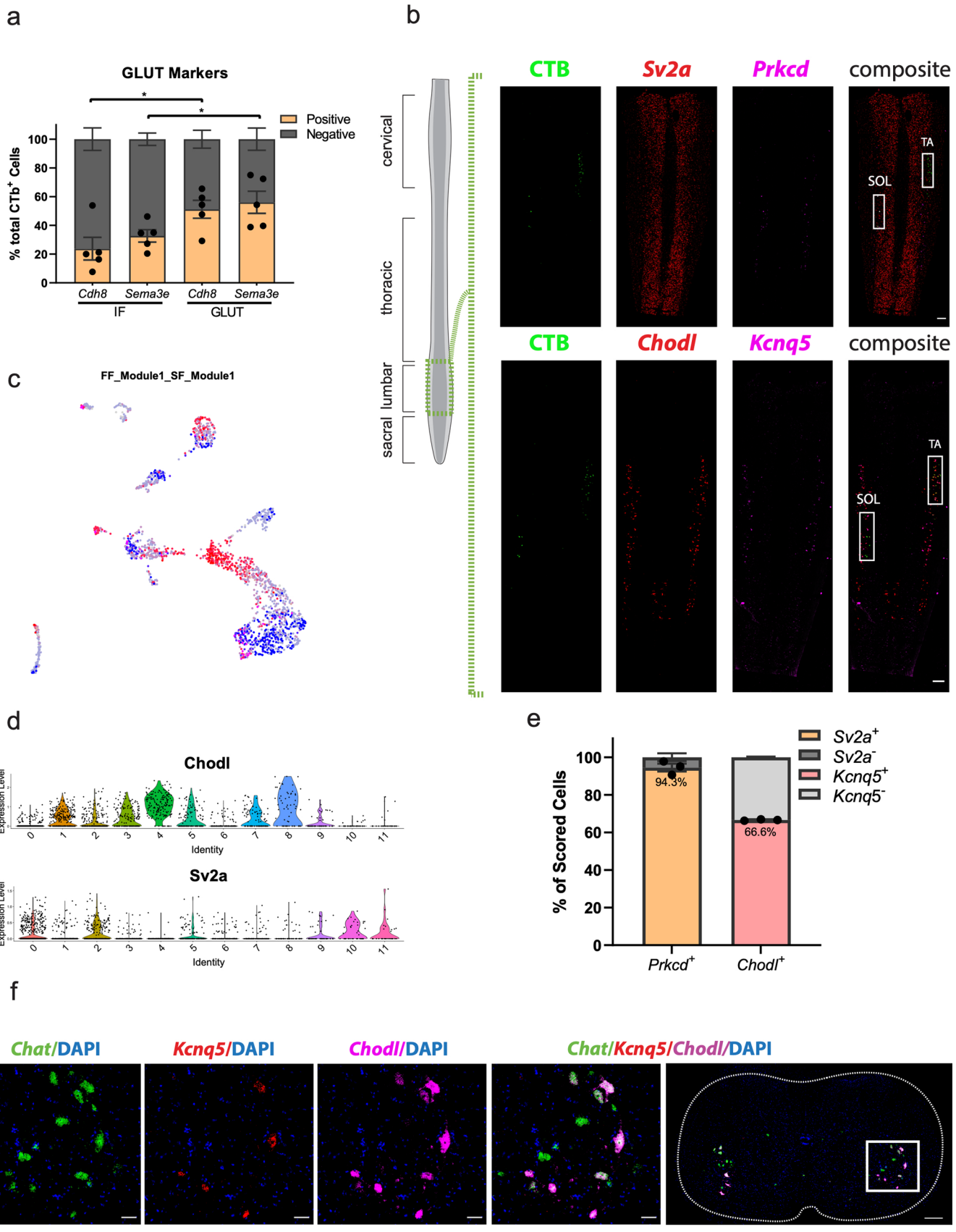

Extended Data Fig. 6 | See next page for caption.

Extended Data Fig. 6 | Retrograde CTB labeling of motor pools connects transcriptional subpopulations with motor pools. a, Proportion of CTB-labeled cells from GLUT and IF that are labeled with *Cdh8* and *Sema3e*. The GLUT has a significantly larger proportion of *Cdh8* + and *Sema3e* + cells than the IF. n = 5 biologically independent animals. **b**, Lower power view of *in situ* hybridization against *Prkcd/Sv2a*, and *Kcnq5/Chodl* (insets=Fig. 4h) in longitudinal sections demonstrates the specificity of CTB injections into the *Soleus* (SOL) and *Tibialis anterior* (TA). n = 5 (TA) and 4 (SOL) biologically independent animals. One-way ANOVA with post-hoc Sidak multiple comparison test between same-gene conditions. Adjusted p-values=0.0212 (*Cdh8*) and 0.0499 (*Sema3e*). **c**, Expression of FF and SF gene modules overlaid on UMAP of all α motor neurons. **d**, Average log-normalized canonical marker expression of *Chodl* (fast-firing) and *Sv2a* (slow-firing). Scale bars = 250 μm. **e**, Proportion of *Prkcd* + cells positive for *Sv2a* (left) and proportion of *Chodl* + cells that are positive for *Kcnq5* (right). n = 3 biologically independent animals. **f**, Representative *in situ* hybridization showing *Kcnq5* is expressed in a subset of *Chodl* + cells. n = 4 biologically independent animals. Scale bar=50 μm inset and 200 μm overview. *=p value<0.05, **=p value <0.01, ***=p value<0.001, ****=p value<0.0001. Error bars are SEM.

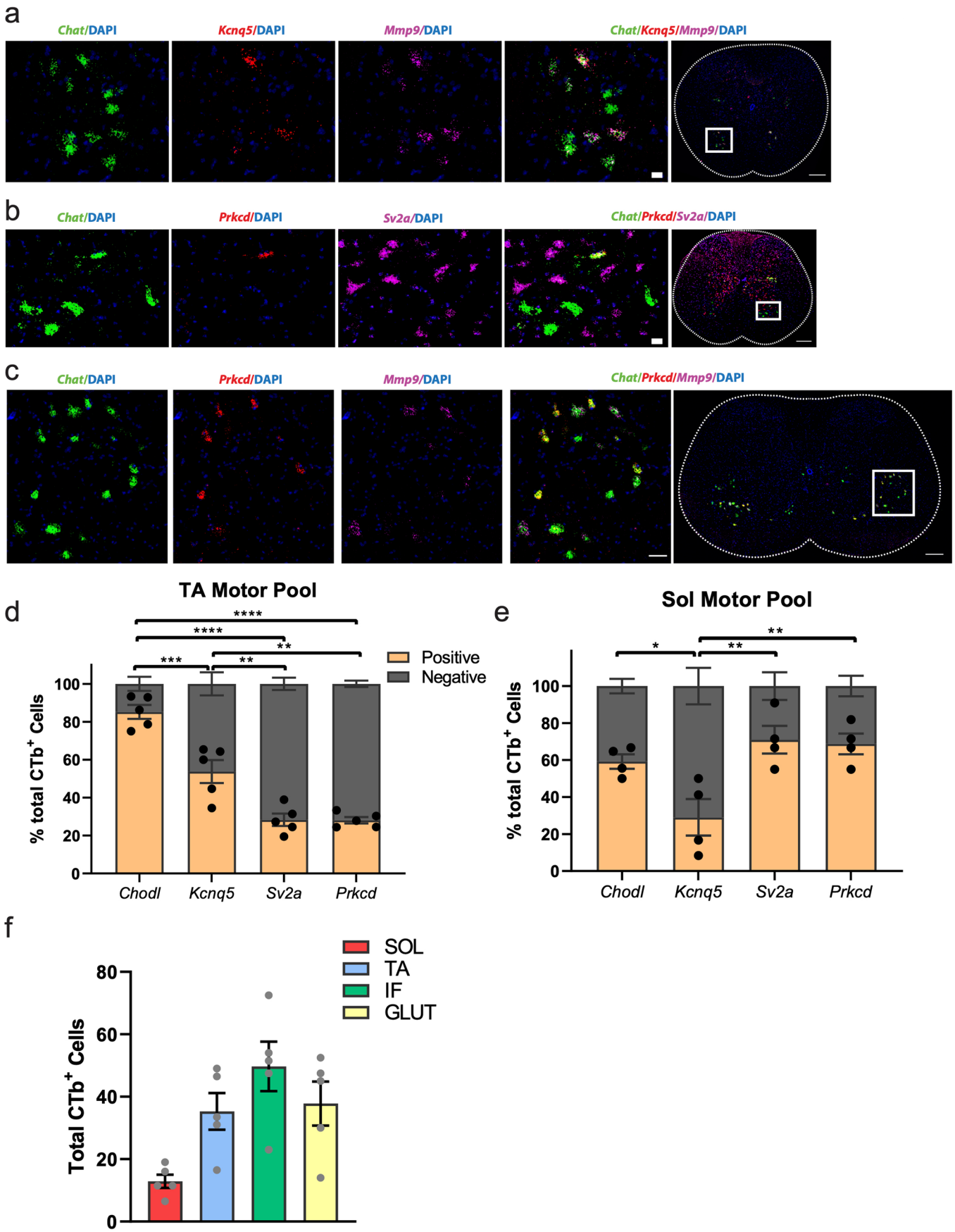

Extended Data Fig. 7 | See next page for caption.

Extended Data Fig. 7 | Retrograde CTB labeling of motor pools enables the identification of transcriptionally distinct classes of fast and slow-firing motor neurons in the adult spinal cord. a, Representative *in situ* hybridization against *Chat/Mmp9/Kcnq5* in transverse spinal cord shows that *Kcnq5* is expressed in a subset of *Mmp9* + fast-firing motor neurons. n = 4 biologically independent animals. Scale bar=20 μm inset and 200 μm overview. **b**, Representative *in situ* hybridization against *Chat/Sv2a/Prkcd* in transverse spinal cord shows that *Prkcd* is expressed in almost every *Chat* + */Sv2a* + slow-firing motor neuron. n = 2 biologically independent animals. Scale bar=20 μm inset and 200 μm overview. **c**, Representative *in situ* hybridization against *Chat/Mmp9/Prkcd* in transverse spinal cord shows that *Prkcd* is excluded from almost every *Chat* + */Mmp9* + fast-firing motor neuron. n = 4 biologically independent animals. Scale bar=30 μm inset and 200 μm overview. **d-e**, Proportion of cells expressing fast and slow-firing markers in the CTB-labeled TA (**d**) and SOL (**e**) motor pools. There is a significantly higher proportion of cells expressing both known and novel fast-firing markers in TA than SOL (**d**), and a higher proportion of cells expressing both known and novel slow-firing markers in SOL than TA. Adjusted p-value=0.0456 (*Chodl* + >*Kcnq5* +). **f**, Total number of CTB-positive cells labeled across biologically independent animals. One-way ANOVA with post-hoc Tukey multiple comparison test among all conditions. n = 4-5 biologically independent animals (**d**-**f**). *=p value<0.05, **=p value <0.01, ***=p value<0.001, ****=p value<0.0001. Error bars are SEM.

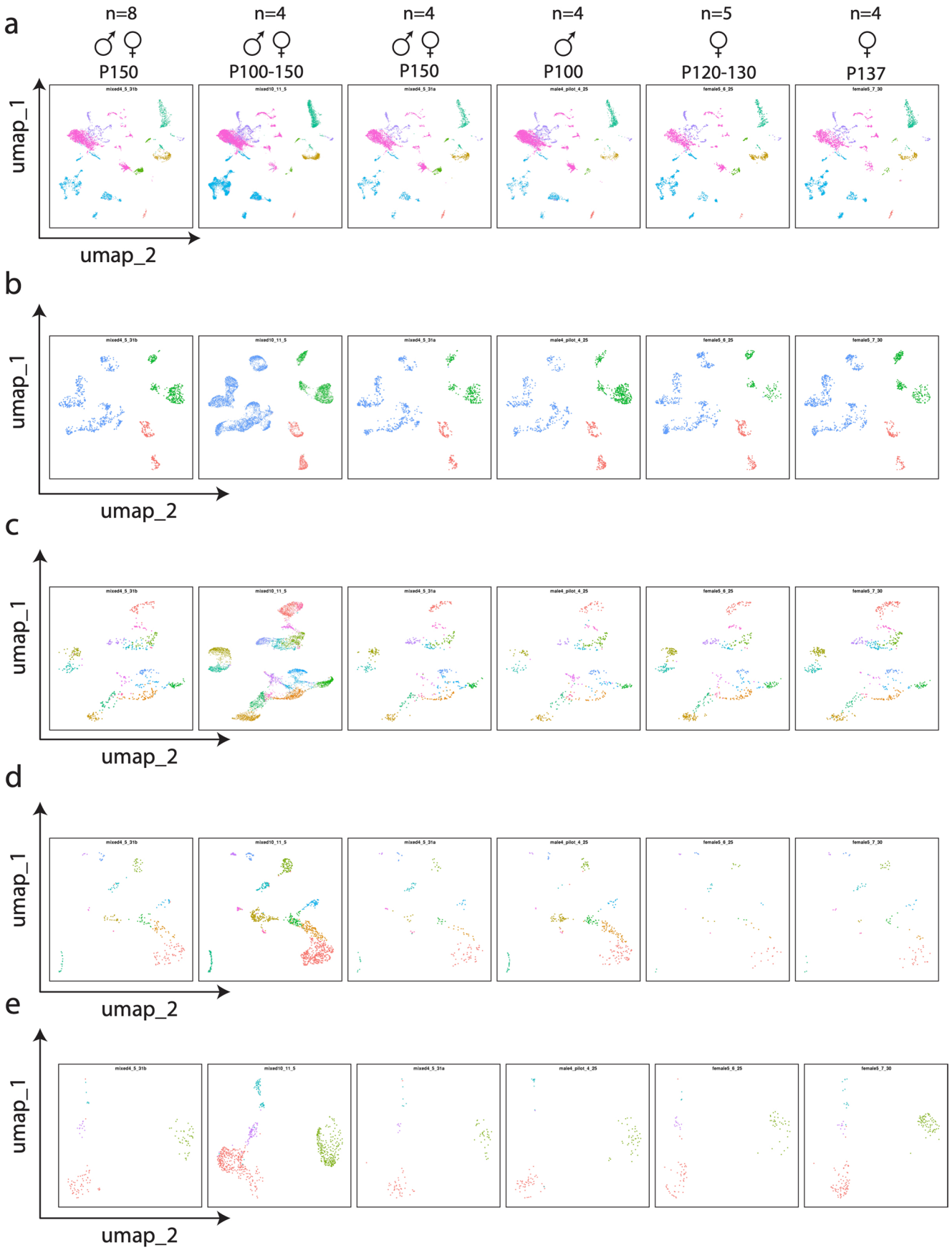

Extended Data Fig. 8 | See next page for caption.

Extended Data Fig. 8 | Cross-replicate variability in single-nucleus transcriptomic experiments. a-e, Each spinal cord sequencing replicate, plotted side-by-side and visualized by UMAP. Note that we observe minimal batch-to-batch variability along sex, age, or replicate number axes in terms of cluster identification and overall shape of the dimensionality reduced data. This does not preclude sex or age-related transcriptional changes but demonstrates that they do not fundamentally alter the transcriptomic classes that we focus on in the manuscript.

nature research

Corresponding author(s): Aaron Gitler

Last updated by author(s): 11/29/2020

Reporting Summary

Nature Research wishes to improve the reproducibility of the work that we publish. This form provides structure for consistency and transparency in reporting. For further information on Nature Research policies, see our Editorial Policies and the Editorial Policy Checklist.

Statistics

For all statistical analyses, confirm that the following items are present in the figure legend, table legend, main text, or Methods section.

n/a	Confirmed	
☐	☒	The exact sample size (*n*) for each experimental group/condition, given as a discrete number and unit of measurement
☐	☒	A statement on whether measurements were taken from distinct samples or whether the same sample was measured repeatedly
☐	☒	The statistical test(s) used AND whether they are one- or two-sided *Only common tests should be described solely by name; describe more complex techniques in the Methods section.*
☒	☐	A description of all covariates tested
☐	☒	A description of any assumptions or corrections, such as tests of normality and adjustment for multiple comparisons
☐	☒	A full description of the statistical parameters including central tendency (e.g. means) or other basic estimates (e.g. regression coefficient) AND variation (e.g. standard deviation) or associated estimates of uncertainty (e.g. confidence intervals)
☐	☒	For null hypothesis testing, the test statistic (e.g. *F*, *t*, *r*) with confidence intervals, effect sizes, degrees of freedom and *P* value noted *Give P values as exact values whenever suitable.*
☒	☐	For Bayesian analysis, information on the choice of priors and Markov chain Monte Carlo settings
☐	☒	For hierarchical and complex designs, identification of the appropriate level for tests and full reporting of outcomes
☒	☐	Estimates of effect sizes (e.g. Cohen's *d*, Pearson's *r*), indicating how they were calculated

Our web collection on statistics for biologists contains articles on many of the points above.

Software and code

Policy information about availability of computer code

Data collection	No software was used for data collection.
Data analysis	Python 3: cellranger 3.0 R 3.6.1: XML_3.98-1.20, scales_1.1.0, reshape2_1.4.3, doParallel_1.0.15, iterators_1.0.12, foreach_1.4.7, future_1.15.1, ggpubr_0.2.5, magrittr_1.5, gplots_3.0.1.2, ComplexHeatmap_2.2.0 sets_1.0-18, ggthemes_4.2.0, ggplot2_3.2.1, Seurat_3.1.2

For manuscripts utilizing custom algorithms or software that are central to the research but not yet described in published literature, software must be made available to editors and reviewers. We strongly encourage code deposition in a community repository (e.g. GitHub). See the Nature Research guidelines for submitting code & software for further information.

Data

Policy information about availability of data

All manuscripts must include a data availability statement. This statement should provide the following information, where applicable:

- Accession codes, unique identifiers, or web links for publicly available datasets
- A list of figures that have associated raw data
- A description of any restrictions on data availability

All sequencing data is available in raw and processed form from NCBI-GEO (accession: GSE161621). An interactive web portal for exploring the dataset is available at http://www.spinalcordatlas.org.

Field-specific reporting

Please select the one below that is the best fit for your research. If you are not sure, read the appropriate sections before making your selection.

☒ Life sciences ☐ Behavioural & social sciences ☐ Ecological, evolutionary & environmental sciences

For a reference copy of the document with all sections, see nature.com/documents/nr-reporting-summary-flat.pdf

Life sciences study design

All studies must disclose on these points even when the disclosure is negative.

Sample size	For sequencing experiments, sample size was not pre-calculated (as cell population size was unknown). However, minimum cluster size (>50 nuclei) conforms to typical standards in the field of single-cell analysis. Otherwise, sample size was predetermined without sample-size calculation.
Data exclusions	Nuclei falling below a threshold for number of uniquely mapped transcripts were excluded by cellranger 3.0. Reads obtained from mitochondrial RNA were discarded, as were doublet nuclei (determined in Seurat), all in a blinded fashion. For the CTB experiments, only animals that showed high signal/noise in CTB labeling were used, determined in a blinded fashion.
Replication	All replication of the experiments are reported, either as representative images or quantified replicates.
Randomization	No randomization was performed.
Blinding	Quantification of CTB-labeled in situ microscopy images were quantified in a blinded fashion, described at length in the methods.

Reporting for specific materials, systems and methods

We require information from authors about some types of materials, experimental systems and methods used in many studies. Here, indicate whether each material, system or method listed is relevant to your study. If you are not sure if a list item applies to your research, read the appropriate section before selecting a response.

Materials & experimental systems

n/a	Involved in the study
☐	☒ Antibodies
☒	☐ Eukaryotic cell lines
☒	☐ Palaeontology and archaeology
☐	☒ Animals and other organisms
☒	☐ Human research participants
☒	☐ Clinical data
☒	☐ Dual use research of concern

Methods

n/a	Involved in the study
☒	☐ ChIP-seq
☒	☐ Flow cytometry
☒	☐ MRI-based neuroimaging

Antibodies

Antibodies used	rabbit anti-CTB (Abcam ab34992)
Validation	Validated internally by staining exogenously injected CTB in fixed tissue. Only animals that showed specific labeling in the motor pools and muscles injected were included in the subsequent analysis.

Animals and other organisms

Policy information about studies involving animals; ARRIVE guidelines recommended for reporting animal research

Laboratory animals	Mus Musculus, Chat-IRES-Cre (stock no. 006410m, Jax)/+ ; Nt-Ng (stock no. 023035, Jax)/+ mice aged P100-150, male and female. B6 male and female mice aged P100-150 used for in situ follow-up experiments, male and female.
Wild animals	No wild animals were used in this study.
Field-collected samples	No field collected samples were used in this study.
Ethics oversight	Stanford Administrative Panel on Laboratory Testing (APLAC) protocol: #30643

Note that full information on the approval of the study protocol must also be provided in the manuscript.